



Enhancing the Photoelectric Performance of Photodetectors Based on Metal Oxide Semiconductors by Charge-Carrier Engineering

Weixin Ouyang, Feng Teng, Jr-Hau He,* and Xiaosheng Fang*

Semiconductor-based photodetectors (PDs) convert light signals into electrical signals via the photoelectric effect, which involves the generation, separation, and transportation of the photoinduced charge carriers, as well as the extraction of these charge carriers to external circuits. Because of their specific electronic and optoelectronic properties, metal oxide semiconductors are widely used building blocks in photoelectric devices. However, the compromise between enhancing the photoresponse and reducing the rise/decay times limits the practical applications of PDs based on metal oxide semiconductors. As the behaviors of the charge carriers play important roles in the photoelectric conversion process of these PDs, researchers have proposed several strategies, including modification of light absorption, design of novel PD heterostructures, construction of specific geometries, and adoption of specific electrode configurations to modulate the charge-carrier behaviors and improve the photoelectric performance of related PDs. This review aims to introduce and summarize the latest researches on enhancing the photoelectric performance of PDs based on metal oxide semiconductors via charge-carrier engineering, and proposes possible opportunities and directions for the future developments of these PDs in the last section.

1. Introduction

Semiconductor-based photodetectors (PDs) convert light signals into electrical signals via the photoelectric effect. Promoted by the progressive nanoscience and nanotechnology, PDs have achieved prolonged developments in last decades.^[1] To meet

the ever-changing and developing requirements from the fundamental research and industrial applications, including space communications^[2] and flame detection,^[3] the photoelectric properties of PDs based on low-dimensional nanostructures require further improvements, which focus on the adoption of appropriate sensitive semiconductor materials and the optimization of device configurations.


Metal oxide semiconductors are useful building blocks in the photoelectric devices for their specific electronic and optoelectronic properties. Their low-dimensional nanostructures with suitable bandgap, unique conduction properties, and confined carrier conduction pathways made them suitable candidates for sensitive materials in photoelectric devices. Besides, metal oxide semiconductor nanostructures are stable and easy to be prepared and processed, which make them promising for assembling high-performance PDs in large scale. For photoconductive-

type PDs based on commonly used metal oxide semiconductor nanostructures such as ZnO and SnO₂, they can exhibit high absorption coefficient and high response resulted from the pronounced surface effects.^[4] However, these surface effects also cause the slow response speed of these PDs, which is related to the oxygen absorption/desorption process at the surface of oxide semiconductors. In the dark, the oxygen molecules absorb on the oxide surface by capturing the free electrons from the conduction band of these oxide semiconductors, forming a surface depletion layer with low conductivity. Under light illumination, the photogenerated holes migrate to the surface and discharge the negatively charged adsorbed oxygen ions, causing the photodesorption of oxygen molecules from the surface. When the light is off, the oxygen molecules are reabsorbed on the oxide surface and extract the photogenerated electrons in PDs, leading to the decay of current. Thus, the pronounced surface effects lead to the slow oxygen absorption/desorption process at the surface of oxide semiconductors, causing the long rise/decay times of these related PDs.^[5,6] In other cases, the rapid recombination of photogenerated electron-hole pairs (i.e., short-carrier lifetime) and low-absorption coefficient of semiconductor nanomaterials leads to low quantum efficiency and poor photodetection performance.^[7,8] The compromise between enhancing the responsivity and reducing the rise/decay times

Dr. W. X. Ouyang, Prof. X. S. Fang
Department of Materials Science
Fudan University
Shanghai 200433, P. R. China
E-mail: xshfang@fudan.edu.cn

Dr. F. Teng
School of Physics
Northwest University
Xi'an 710127, P. R. China

Prof. J.-H. He
Computer
Electrical and Mathematical Sciences and Engineering (CEMSE) Division
King Abdullah University of Science and Technology (KAUST)
Thuwal 23955-6900, Kingdom of Saudi Arabia
E-mail: jrhou.he@kaust.edu.sa

 The ORCID identification number(s) for the author(s) of this article can be found under <https://doi.org/10.1002/adfm.201807672>.

DOI: 10.1002/adfm.201807672

seriously limits the practical applications of PDs based on metal oxide semiconductors.^[9] To deal with this problem, it is necessary to track the behaviors of carriers in these PDs and clarify their influences on the photoelectric properties.

In general, the photoelectric conversion processes from optical signals to electric signals via semiconductor-based PDs mainly involve four steps:

- 1) *Generation of the Charge Carriers*: When the incident photons are absorbed by the semiconductors after the light trapping process, the photo-excited electrons transit from the valence band (VB) to the conduction band (CB) of the semiconductors, while the corresponding holes are left in the VB. The obtained electrons in the CB and holes in the VB are recognized as the photoinduced carriers.
- 2) *Separation of the Charge Carriers*: Forced by the applied electric field or built-in electric field formed at the interface of heterojunctions, the photoinduced electron–hole pairs are separated and move toward different electrodes.
- 3) *Transportation of the Charge Carriers*: After being separated, the different charge carriers would travel along the conduction pathways toward alternative electrodes, where the tapping and recombination of charges carrier occur and cause decreased photoelectric conversion efficiency.
- 4) *Extraction of the charge Carriers*: After the charge carriers arrived at the electrodes, in accordance with the varied electrode configurations, they will be extracted and conducted to the external circuit, which contribute to the photocurrent.

The photoelectric performance of PDs relates with the behaviors of these charge carriers. The implement of charge-carrier engineering, including the generation of increased amount of photoinduced electron–hole pairs resulted from enhanced photo absorption, the effective separation of the chare carriers driven by the applied or inner electric fields at junctions, as well as the efficient transport and extraction of charge carriers promoted by the superior device structures, leads to the modulation of charge-carrier behaviors and promotes the improved photoelectric performance of PDs.

“5S” is a standard rule for high-performance optoelectronic devices, which stands for high sensitivity, high spectral selectivity, high signal-to-noise ratio, high speed, and high stability.^[1,10] To meet with these requirements and rectify the low photoresponse and slow response speed of metal oxide semiconductor–based PDs, researchers have proposed several strategies, such as modification of light absorption, utilization of defects engineering, development of novel PD heterostructures, construction of specific geometries, and adoption of specific electrode configurations, to achieve enhanced responsivity and accelerated response speed. Full considerations should be taken while applying these strategies so as to meet the different aspects of the “5S” standards. Taking the defect engineering in PDs as an example, similar to its applications in solar cells and photocatalysts,^[11,12] the considerate defect engineering in PDs can improve the light absorption and prolong the photo-carrier lifetime, leading to good sensitivity, high responsivity, and even extended photoresponse range.^[13,14] The emergence of defect-induced trap states can shorten the response times via the promoted recombination of photogenerated charge carriers. Moreover, the significant reduction of dark current could

realize the enhanced specific detectivity. Thus, the controlled defect engineering of trap states can endow PDs with both high responsivity and fast response.^[15]

This paper aims to provide a brief, systematical, and comprehensive introduction of the latest researches on enhancing the photoelectric performance of metal oxide semiconductor–based PDs via charge-carrier engineering, and possible opportunities and directions for the future developments of these PDs are proposed in the last section.

2. Generation of the Charge Carriers

The generation of photoexcited carriers upon the absorption of photons is the leading process of photoelectronic detection, and it has primary impacts on the photoelectric conversion process. In order to enhance the concentration of photogenerated electrons and holes, increasing the light absorption of active semiconductor materials in the PD should be taken into considerations. The construction of special structures, doping, and taking advantages of the surface plasma resonance effect, the hot electron injection effect and the multiple excitons effect are commonly used methods to enhance the light absorption.

2.1. Light-Harvesting Structures

Adjusting the surface roughness for the precise control of light scattering, transmission, and reflection is frequently utilized to enhance the light absorption in the optical devices, including solar cells and PDs.^[16–18] Generally, nanostructures at the device surface exhibit excellent photon capturing and confinement abilities to enhance light absorption and improve forward scattering of incident light. Better photon management by employing the nanostructures allows for thinner active layers in the PDs, which not only reduces the cost and amount of material used, but also decreases the electrical loss during the photocarrier transport.^[19] Recently, a Ω -shaped 1D SnO_2 @ZnO PD with electrospun SnO_2 nanofibers as core and ultrathin ZnO film as shell has been reported. It exhibits a high photo-to-dark current ratio of up to 10^4 at around 280 nm.^[20] As demonstrated by both theoretical simulations and experimental comparisons, the unique compact Ω -shaped nanostructure does contribute to photon trapping and gaining process, especially in the back-illumination configuration. **Figure 1a,b** shows the optical field distribution under face and back illumination via finite-difference time domain (FDTD) simulation. The Ω -shaped structure is proved to be more effective for trapping light illuminated from the back side. Once the light is trapped inside the structure, it will certainly increase the photon absorption, thus leading to improved photoelectric properties.

2.2. Doping

Energy band engineering is also considered as an effective method to enhance the light absorption and extend the absorption spectrum. Due to its simplicity and controllability, doping is frequently utilized to modulate the band structure of metal oxide

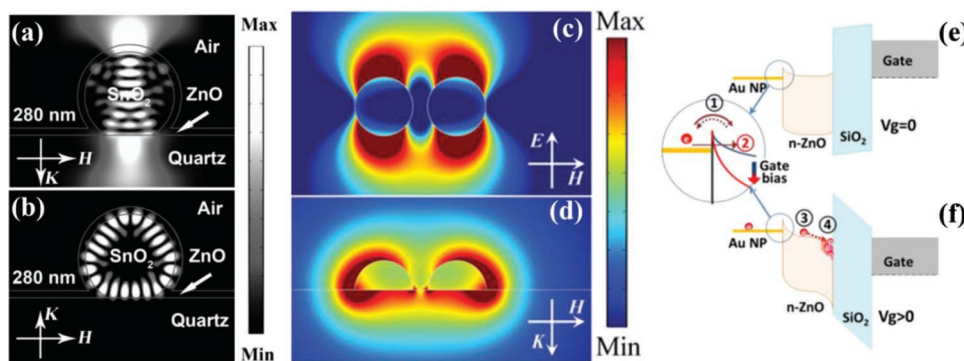


Figure 1. a,b) The optical field distribution of Ω -shaped $\text{SnO}_2@ZnO$ nanostructure under face and back illumination simulated by FDTD. c,d) The electric-field-intensity distribution of Au/Se hybrid structure under 600 nm light illumination from the top view and side view. e,f) Internal field-assisted hot electron migration and quantum tunneling at the interface of Au/ZnO hybrid structure with different gate voltage biases. a,b) Reproduced with permission.^[20] Copyright 2017, Wiley-VCH. c,d) Reproduced with permission.^[29] Copyright 2016, Wiley-VCH. e,f) Reproduced with permission.^[36] Copyright 2016, American Chemical Society.

semiconductors. The introduction of dopants into semiconductors causes the formation of impurity energy level and the shift of absorption edges toward longer wavelength. Therefore, the photoelectric properties of PDs based on the doped metal oxide semiconductors are largely affected. Dutta et al. prepared sol-gel ZnO films with p-type conductivity by doping and codoping with N and Al-N, respectively.^[21] Compared with the undoped and codoped films, the N-doped film exhibits better response to UV light. Young and Liu fabricated an indium-doped ZnO nanostructure UV PD uniformly on a glass substrate, which exhibited high sensitivity, fast response speed, and good orientation properties.^[22] At 1 V bias, the indium-doped ZnO PD achieves an on/off ratio of 740 at 365 nm and exhibits the short rise/decay times of 3.02/1.53 s. When irradiated with 360 nm light, this PD displays a UV-vis rejection ratio of ≈ 312 . In general, the trap states induced by doping could promote the recombination of charge carriers, which would lead to shortened response times. Shabannia synthesized vertical Co-doped ZnO nanorod arrays on a flexible polyethylene naphthalate (PEN) substrate and assembled them into a metal-semiconductor-metal (MSM)-type UV PD.^[23] At 5 V bias, this UV PD exhibits a calculated responsivity of 8.76 A W^{-1} , a photosensitivity of 250, and very short rise/decay times of 0.229/0.276 s. Though doping can enhance the light absorption of metal oxide nanostructures and improve their photoelectric properties, and excess amounts of dopants could become the trapping and recombination centers of photogenerated charge carriers, which would weaken the photoresponse of PDs instead.^[24]

2.3. Surface Plasma Resonance Effect

Localized surface plasmon resonance (LSPR) is described as the photoexcitation-induced collective oscillations of free charges confined in a highly conductive nanocrystal.^[25] In recent years, metal nanocrystals (such as Au, Ag, and Cu) with LSPR effects have received worldwide attentions for their intriguing optical properties and versatile technological applications. The absorption and scattering cross-sections of these metal nanostructures can be tailored over a broad wavelength region from UV and visible to infrared (IR) wavelengths via changing the size, shape,

metal composition, and environment.^[26] By taking advantage of the light-confinement effect and tunable light absorption, various plasmonic PDs that combine low-dimensional semiconductor nanostructures and these plasmonic metal nanocrystals have demonstrated excellent plasmon-enhanced device performance.^[27,28] Our group achieved broadband responsivity enhancement of single Se microtube (Se-MT) PDs in the UV-vis region by the modification of different metal nanoparticles (NPs).^[29] The pristine Se-MT PD demonstrates broadband photoresponse from 300 to 700 nm with a peak responsivity of about 19 mA W^{-1} at 610 nm and short rise/decay times of 0.32/23.02 ms. After the deposition of Au NPs with optimal sizes and densities on the surface, the Au-NP-decorated Se-MT PD achieves broadband responsivity enhancement (≈ 600 – 800%) resulting from both the surface modification and surface plasmon coupling. Figure 1c,d shows the electric-field-intensity distribution of Au/Se hybrid structure under 600 nm light illumination in the top view and the side view, this simulation result further confirms that the LSPR effect can enhance the light absorption of this hybrid structure.

Targeting at the defined absorption range and low light absorption of metal oxide semiconductors, the LSPR effect can significantly improve the photoelectric performance of PDs based on metal oxide materials. Tian et al. prepared an MSM-structured UV PD based on a high-quality ZnO thin film grown on a quartz substrate.^[30] The light absorption of ZnO thin film is enhanced partly in the UV region, and the responsivity of the PD is enhanced from 0.836 to 1.306 A W^{-1} after the deposition of Pt NPs on the device surface, revealing the improved photoelectric performance benefiting from the LSPR effect of Pt NPs. Guo et al. prepared MgZnO MSM UV PDs and conducted the surface decoration of Pt NPs.^[31] Due to the enhanced scattering of incident light via the surface plasmons of Pt NPs, the responsivities of all PDs with different electrode spaces (3, 5, and $8 \mu\text{m}$) were enhanced dramatically.

2.4. Hot Electron Injection Effect

Resonant surface plasmons can decay nonradiatively through the generation of hot carriers, and the additional scattering

and relaxation of these high-energy carriers would produce photocurrent in PDs.^[32,33] The generation of hot carriers is not confined by the bandgap of semiconductor, but rather extended to Schottky barrier height or tunnel junction, providing the possibility to detect photons with energies lower than the bandgaps of semiconductors. The hybrid metal–semiconductor system would be an excellent unit for manipulating the emission of hot carriers and a promising platform for fabricating plasmonic PDs with multifunction. These hot-carrier processes can be achieved and regulated via the geometric design of plasmonic nanostructures, the choice of plasmonic material, and the design of plasmonic material–semiconductor interfaces. The deeper exploration and utilization of the hot electron injection effect would pave ways for improved optoelectronic performance.

Ouyang et al. deposited Au NPs on a CdMoO₄–ZnO composite film by the ion sputtering method.^[34] The as-constructed PD with an optimized deposition time of Au NPs yields an approximately twofold higher photocurrent and the decay time reduces by half, as compared with the CdMoO₄–ZnO PD. The hot electrons from Au NPs are injected into the CdMoO₄–ZnO composite film, leading to the increased photocurrent. When the light is off, the Schottky barriers formed between Au NPs and CdMoO₄–ZnO composite film block the carrier transportation and accelerate the decay process of current. Thus, the hot electron effect and the construction of Schottky junctions from the Au NPs contribute to the improved photoelectric performance. Pescaglioni et al. built Au nanorod–ZnO nanowire hybrid systems as a new class of near-IR PDs.^[35] The PD shows large photoresponse between 650 and 850 nm and an “ultrafast” transit time within 250 ms. The quantum efficiency was calculated to be ≈3% at 650 nm, more than 30 times larger than that of the equivalent Au/ZnO planar PDs. The localized surface plasmons from Au nanorods generate hot electrons at the Au–ZnO Schottky barriers. These hot electrons are then injected into the ZnO nanowire which functions as a passive component for charge collection, thus generating the photocurrent. The hot electron generation and injection process contributes to the improved and extended photodetecting performance of this hybrid device.

Direct coupling of electronic excitations of optical energy via plasmon resonances could achieve improved gain and selectivity in various optoelectronic applications. Kim and co-workers reported a thin ZnO film transistor incorporated with Au nanostructure for plasmon resonance energy detection and electric conversion.^[36] This plasmonic Au–ZnO field effect transistor (FET)-type PD collects the plasmonic-induced hot electrons from the physically isolated Au nanostructures, which contributes to the amplification of drain current. Figure 1e,f displays the typical migration process of hot electrons at the interface of Au/ZnO hybrid structure with different gate voltage biases. It can be deduced that an electron accumulation layer is generated under positive gate bias, which can modulate the behaviors of charge carriers in the ZnO-based FET. Highly efficient collection and amplification of hot electrons are achieved by the internal electric field and quantum tunneling effect at the Au–ZnO junction. In addition, the versatility of plasmonic nanostructures in wavelength tunability endows this device architecture an ultrawide spectral response.

2.5. Multiple Excitons Effect

Generally, one photon excitation can only produce a single electron–hole pair, which implies that the conversion efficiency from photons to electron–hole pairs can hardly reach a hundred percent. However, after the absorption of a photon bearing at least twice the bandgap energy, the multiple exciton generation effect occurred in semiconductor nanocrystals or quantum dots induces the generation of two or more electron–hole pairs from a single absorbed photon.^[37] The trapping of electrons at the quantum-dot surfaces leaves behind long-lived holes that are able to circulate through the photoconductor and external circuit multiple times before the recombination with holes. The conversion efficiency from photons to electron–hole pairs in these devices can exceed 100%.^[38] The generation of multiexcitons in these systems happens within 200 fs, which reveals that it is an instantaneous event. This multiple exciton generation effect should lead to great improvements in the photoresponse of PDs.^[39]

3. Separation of the Charge Carriers

Heterojunctions formed between different semiconductor materials have extensive applications in solar cells, photoelectrochemical (PEC) cells, PDs, and other photovoltaic devices due to their profound influences on electronic properties and potentials in multifunction and property tuning. Heterojunctions can create built-in electric fields at the interfaces, which efficiently separate photogenerated electron–hole pairs and regulate the transportation of carriers in photoelectric devices. Referring to the different conduction types of various components in heterojunctions based on metal oxide semiconductors, we classify the heterojunctions into n–n, p–n, p–i–n, and Schottky junctions generally.

3.1. n–n Junction

If the potential values of the conduction band and valence band edges of n-type semiconductor A are more negative than those of another n-type semiconductor B, a type-II heterojunction can be formed between these two n-type semiconductors. Several suitable n-type semiconductors have been utilized to improve the photoelectric properties of ZnO-based PDs.

Our group prepared a novel CdMoO₄–ZnO composite film by spin-coating CdMoO₄ microplates on ZnO film and constructed this composite film into a heterojunction PD.^[34] The device structure of this PD is shown in Figure 2a. With an optimized loading amount of CdMoO₄ microplates, this composite film PD achieves an ≈18-fold higher responsivity than the pure ZnO film PD at 350 nm with a bias of 5 V bias (Figure 2b), and its decay time shortens to half of the value of the ZnO film PD. It is demonstrated that the introduced CdMoO₄ microplates form type-II heterojunctions with the ZnO film, which leads to improved photoelectric performance.

ZnO nanostructures can also be used to modify the photoelectric properties of other metal oxide semiconductors. Li et al. fabricated UV heterojunction PDs based on ZnO quantum

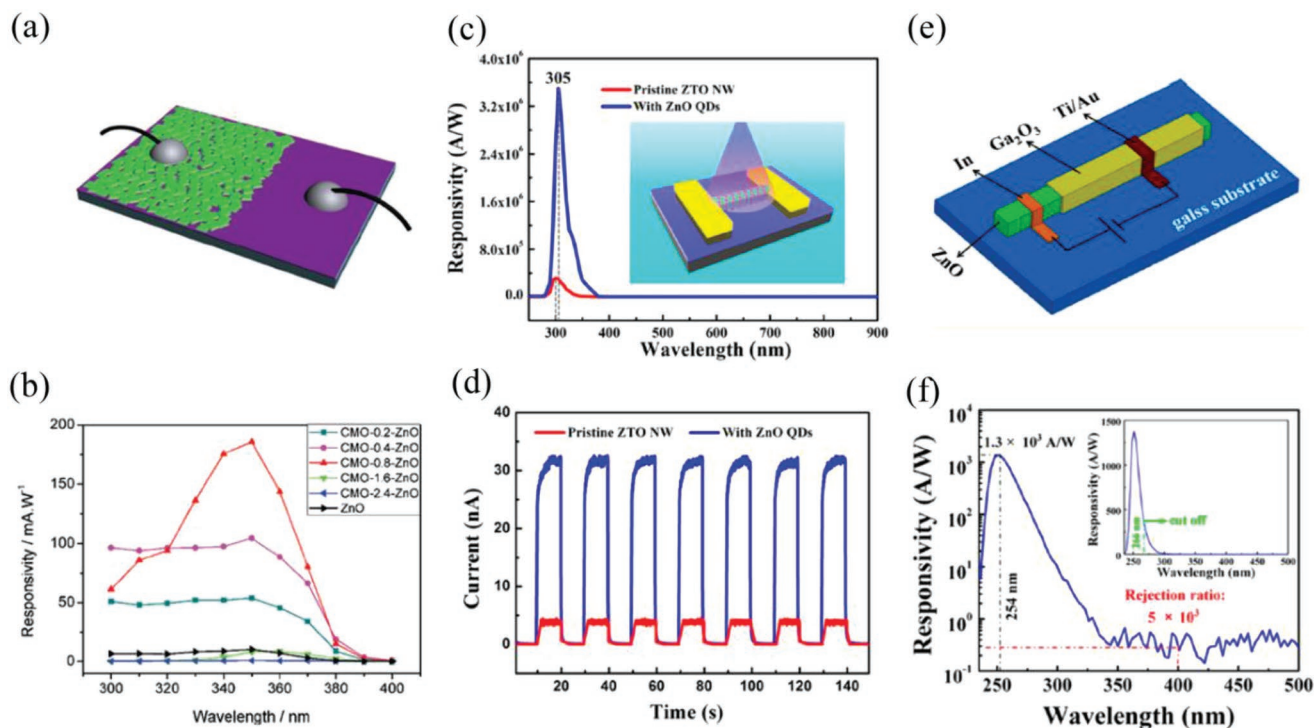


Figure 2. a) Schematic diagram of the CMO–ZnO PD. b) Spectral response of the CMO–ZnO PDs and ZnO PD at 5 V bias. c) Spectral responsivity of the ZTO NW PD and the ZnO QD decorated ZTO NW PD at wavelength range from 250 to 900 nm at a bias voltage of 1 V. The inset is the schematic illustration of the as-fabricated PD. d) Time-domain photoresponse of two kinds of PDs at 1 V with a light intensity of $0.67 \mu\text{W cm}^{-2}$. e) Schematic diagram of the ZnO–Ga₂O₃ core–shell microwire APD device. f) Spectral response of the device at -6 V bias. a,b) Reproduced with permission.^[34] Copyright 2017, Wiley-VCH. c,d) Reproduced with permission.^[40] Copyright 2017, American Chemical Society. e,f) Reproduced with permission.^[43] Copyright 2015, American Chemical Society.

dot-decorated Zn₂SnO₄ nanowires.^[40] The optimized hetero-junction PD displays an ultrahigh on-off ratio of up to 6.8×10^4 , a specific detectivity of up to 9.0×10^{17} Jones, and a photoconductive gain of up to 1.1×10^7 . It also presents fast response speed and excellent stability. Compared with a pristine nanowire, this quantum dot-decorated Zn₂SnO₄ nanowire demonstrates about 10 times higher photocurrent and responsivity (Figure 2c,d). Their high performance originates from the rational energy band alignment engineering, which allows efficient separation of electron–hole pairs at the interfaces.

The potential differences between the conductive band edges of n-type semiconductors in n–n junctions are usually smaller than the differences between n-type and p-type semiconductors in the p–n junction, thus resulting a weaker driving force for the separation and transport of photogenerated electron and hole pairs. The avalanche effect can be utilized to remedy these drawbacks of the n–n junction and achieve high-performance PDs.^[41] The avalanche effect occurs when a large external electrical field is applied to a semiconductor system to accelerate the charge carriers to sufficiently high energy that they can generate additional electron–hole pairs through collisional ionization, leading to strongly amplified photoresponse of PDs. Avalanche PDs rely on the avalanche effect of heterojunction at high reverse bias, and usually exhibit very high photosensitivity and fast response speed, which are able to detect weak or fast changing signals.

Chen et al. grew single crystalline α -Ga₂O₃ epilayers on nonpolar ZnO (1120) substrates and demonstrated a high-performance

Au/ α -Ga₂O₃/ZnO isotype heterostructure-based Schottky barrier avalanche diode.^[42] The device exhibits self-powered characteristics with a dark current lower than 1 pA, a high UV–vis rejection ratio of 10^3 , and a detectivity of 9.66×10^{12} Jones. It also generates high avalanche gains over 10^3 and a low ionization coefficient ratio of electrons and holes, leading to a total gain over 10^5 and a high responsivity of $1.10 \times 10^4 \text{ A W}^{-1}$, while the layered device structure leads to a relatively long decay time of 238 μs . To accelerate the response speed, Zhao et al. fabricated highly crystallized ZnO–Ga₂O₃ core–shell microwires into high-performance solar-blind avalanche PD. The device structure of this PD is depicted in Figure 2e.^[43] It displays a high responsivity of up to $1.3 \times 10^3 \text{ A W}^{-1}$ at -6 V bias (Figure 2f), a high detectivity of 9.91×10^{14} Jones, and ultrashort response times of 20/42 μs . Surprisingly, its photoelectric performance in solar-blind waveband is comparable to or even higher than that of the commercial Si avalanche PD (APD) (APD120A2 from Thorlabs Inc.), which makes this core–shell heterostructure highly promising for practical solar-blind PDs.

3.2. p–n Junction

As the most ubiquitous and fundamental building block of modern electronics, p–n junctions play a crucial role in modern microelectronics applications, including integrated circuits, sensors, solar cells, and lasers.^[44] Owing to the photovoltaic

effects resulted from p–n junctions, photoexcited electron–hole pairs generated at the p–n junctions are separated by the built-in electric field. The photoelectrical response speed of the p–n junction is dominated by the drift time of carriers inside the depletion area of the junction, which differs from the long-time photoconductive relaxation of metal oxide semiconductor nanostructures originating from the adsorbates on their surface. Thus, the adoption of the p–n junction in photoelectric devices can achieve improved photoresponse and fast response speed.

In recent years, nanostructured p–n and p–i–n junctions made from low-dimensional metal oxide nanostructures with various configurations, such as core–shell, axial, crossed, and branched structures, have been fabricated to construct high-performance PDs. p-Type semiconductor materials, as the alternative component in p–n junctions, demonstrate prominent and irreplaceable roles in constructing high-performance photoelectric devices. In order to explore the influences of p–n junctions on the photoelectric properties of metal oxide semiconductor nanostructures, the PDs based on p–n heterojunctions are classified in accordance with the different p-type counterparts (such as inorganic semiconductors and organic semiconductors). Considered the specific optical and electric properties of the inorganic–organic hybrids with perovskites as the representative, the heterojunctions made from the metal oxide semiconductors and perovskites are also presented at the end of this section.

3.2.1. Metal Oxide + Inorganic Semiconductors

Inorganic p-type semiconductors usually possess stable structures, controllable band level structure and predictable characteristics, which can be adopted to construct high-performance optoelectronic devices with common metal oxide semiconductors. TiO₂ is an intrinsically n-type metal oxide semiconductor with wide indirect bandgap. It is regarded as one of the promising candidates for UV photodetection, while the rapid recombination of photogenerated electron–hole pairs in the TiO₂ nanostructures leads to a low quantum efficiency and poor photodetection performance. BiOCl nanosheets/TiO₂ nanotube arrays heterojunction UV PD with high performance was fabricated by a facile anodization process and an impregnation method.^[45] The device structure of this heterojunction PD is presented in **Figure 3a**. The pure TiO₂ PD exhibits a large dark current ($\approx 10^{-5}$ A), a low on/off ratio (8.5) and slow decay time (>60 s), while the optimized BiOCl/TiO₂ heterojunction PD yields a dramatically decreased dark current (≈ 1 nA) (**Figure 3b**), an ultrahigh on/off ratio (up to 2.2×10^5) and fast decay speed (0.81 s) under 350 nm at -5 V. Moreover, it exhibits an increased responsivity of 41.94 A W⁻¹ (**Figure 3c**), a remarkable detectivity (D^*) of 1.41×10^{14} Jones and a high linear dynamic range of 103.59 dB. The greatly improved photoelectric performance is mainly attributed to the heterojunctions at the interface, which facilitate the separation of photogenerated charge carriers and regulate the transportation of the electrons between electrodes.

ZnO is another well-known n-type metal oxide semiconductor with a large bandgap of 3.37 eV and a large exciton binding energy of ≈ 60 meV. Because of its moderate UV absorption, specific electric properties, high stability and low toxicity, ZnO

nanostructures have been intensively investigated for UV photo-detection. Researchers have prepared p-type ZnO materials via doping and then combined them with n-type ZnO materials to form p–n homojunctions aiming for superior photoelectric properties. Hsu et al. synthesized vertical p-ZnO:Cu/n-ZnO homojunction nanowires (NWs) and whole ZnO:Cu NWs on a ZnO thin film/glass substrate by calcination.^[46] The *I*–*V* curve of p-ZnO:Cu/n-ZnO NWs displays the rectifying characteristics and the value of photocurrent is around 6 times larger than that of the dark current at -5 V. Li et al. prepared another single-crystal p-type ZnO nanowires using P₂O₅ as the dopant source via a chemical vapor deposition method.^[47] An intramolecular p–n homojunction is formed in a single ZnO:P NW and displays an on–off ratio as high as 3.2×10^4 at 325 nm. Vabbina et al. grew a p-doped ZnO nanoshell structure around an n-doped ZnO nanorod and then a homogeneous radial p–n junction in the ZnO core–shell configuration was built.^[48] The fabricated radial p–n junction PD exhibits a high responsivity of 9.64 A W⁻¹ and a low noise equivalent power of 0.573 pW Hz^{1/2} under UV illumination. Other p-type inorganic semiconductors have also been utilized to form p–n junctions with ZnO nanostructures to expect improved photoelectric performance. Flemban et al. fabricated high-quality n-type ZnO nanotubes (NTs) on a p-type Si(100) substrate by pulsed laser deposition (PLD).^[49] The fabricated UV PD demonstrates a superior responsivity of up to ≈ 101.2 A W⁻¹ and short rise/decay times of 0.44/0.59 s under 365 nm UV illumination (1 mW cm⁻²) at -5 V. This superior photoelectric performance is attributed to the p–n junction, the high density of photoinduced charge carriers, and the high crystallinity and special geometry of ZnO NTs. In coordination with popular 2D materials, Lee et al. developed a mixed-dimensional 1D ZnO NW–2D WSe₂ nanosheet van der Waals (vdW) heterojunction PD.^[50] The ZnO–WSe₂ heterojunction PD with surface passivation of amorphous fluoropolymer shows superior performance with a much enhanced on/off ratio of over 10⁶, an ideality factor of 3.4–3.6, an extended spectral photoresponses from 400 to 950 nm, and even self-powering characteristics at 0 V.

Carbon nanomaterials have been selected to form p–n heterojunction with ZnO nanomaterials to achieve favorable UV photodetection. Cuong et al. fabricated a transparent vertical ZnO NRs array/thin GO:CNT hybrid film p–n heterojunction device.^[51] This device displays high rectifying characteristics, enhanced UV light absorption and high UV light response. Its photoelectric performance can be further improved by optimizing the GO:CNT ratio and aspect ratio of ZnO NRs. Li et al. combined a semitransparent film of p-type semiconducting single-walled carbon nanotubes (SC-SWNTs) with a molecular beam epitaxy-grown n-ZnO layer to build a vertical p-SC-SWNT/n-ZnO heterojunction UV PD. The device structure is shown in **Figure 3d**.^[52] This device exhibits a low dark current, a current rectification ratio of 10³, and a photoresponsivity up to 400 A W⁻¹ in the UV region from 370 to 230 nm. The detector is practically visible–blind with a high UV-to-visible rejection ratio of 10⁵ due to extremely short photocarrier lifetimes in the 1D SWNTs. In **Figure 3e**, the p-SC-SWNT/n-ZnO heterojunction device shows a relatively fast onset of the photocurrent followed by a slow approach to saturation. The rise/decay times are calculated to be 14/23 s, respectively. Under the same conditions, the In–ZnO–In device in **Figure 3f** shows a significant nonzero

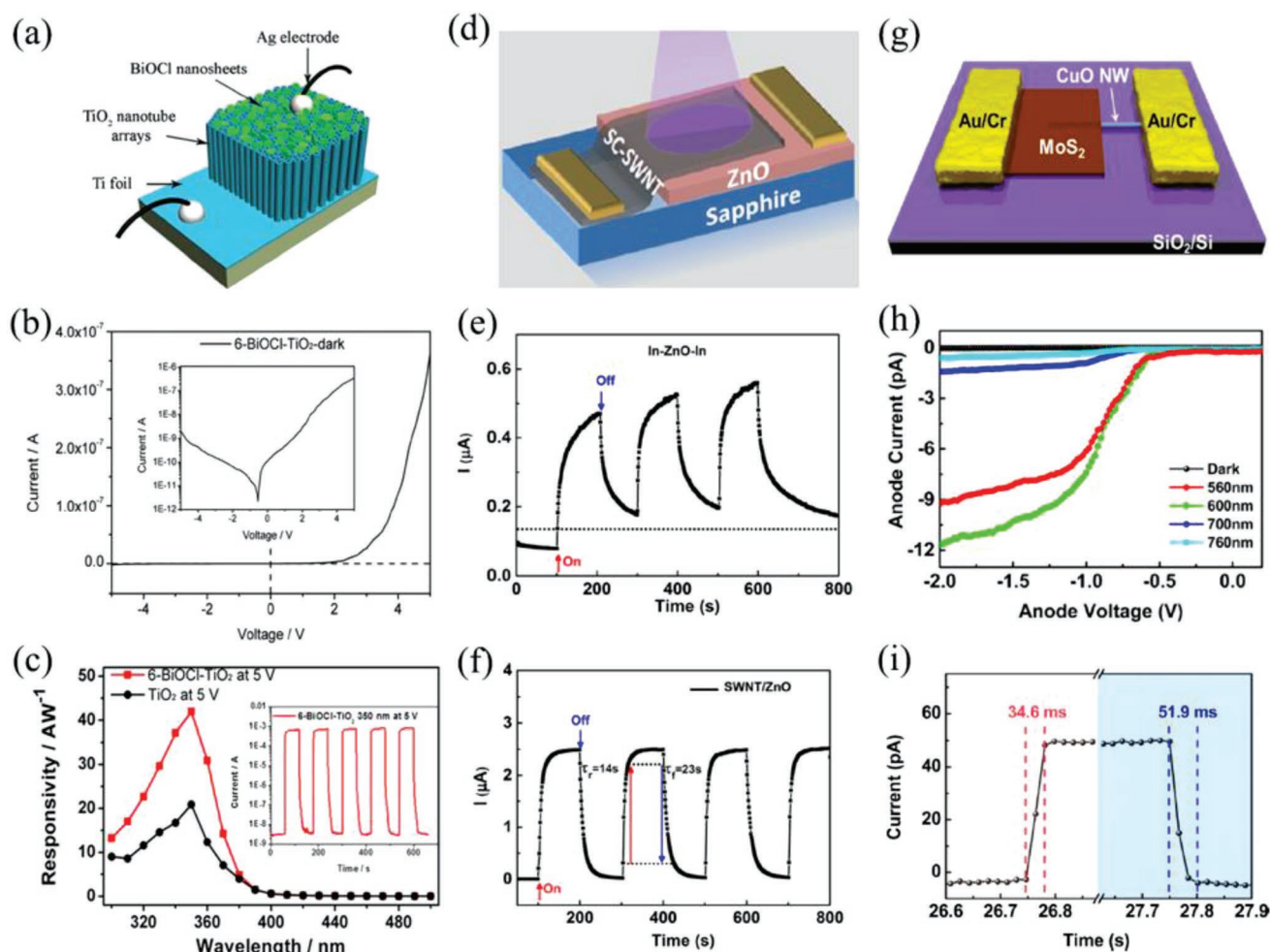


Figure 3. a) Schematic diagram of the BiOCl–TiO₂ UV PD. b) *I*–*V* curves for the device in the dark. c) Spectral response of the TiO₂ PD and the optimized BiOCl–TiO₂ heterojunction PD at –5 V bias. The inset shows the *I*–*t* characteristics of the 6-BiOCl–TiO₂ PD at 350 nm under –5 V bias. d) Schematic of the p-SC-SWNTs/n-ZnO heterojunction under UV irradiation. e, f) Temporal photoresponse of the In–ZnO–In lateral device and the p-SC-SWNT/n-ZnO heterojunction device under 370 nm light at a bias of –2 V. g) Schematic image of the MoS₂/CuO nanosheet-on-1D heterojunction photodiode. h) Photocurrents curves of the MoS₂/CuO photodiode under light illumination of different wavelengths (560, 600, 700, and 760 nm) at 1 mW power and dark conditions. i) Photoresponsive rise and decay times of the MoS₂/CuO photodiode at –2 V under 570 nm light illumination with $P_{\text{light}} = 1.4$ mW. a–c) Reproduced with permission.^[45] Copyright 2018, Wiley-VCH. d–f) Reproduced with permission.^[52] Copyright 2017, American Chemical Society. g–i) Reproduced with permission.^[55] Copyright 2016, American Chemical Society.

dark current, an ≈ 6 times smaller amplitude of the current modulation, and long rise/decay times exceeding 100/600 s, respectively. It is inferred that the introduction of the SWNT/ZnO heterojunction not only enhances the photoresponse but also achieves faster response speed in comparison with the lateral In–ZnO–In device.

p-Type metal oxide semiconductors (such as NiO and CuO) have also been utilized to form p–n heterojunctions with n-type semiconductors to optimize the photodetecting performance. With the solution-processed p-type NiO and n-type ZnO films as sensitizing materials, Kim et al. fabricated an all-inorganic p–n NiO/ZnO heterojunction UV PD.^[53] Thanks to the interfacial trap-induced charge injection that occurs at the ITO/NiO interface by photogenerated holes trapped in the NiO film, the PD achieves a high gain (EQE) of 25 300%. Moreover, Xie et al. fabricated solution-processed p–n heterojunction photodiodes based on NiO/Zn_{1–x}Mg_xO ($x = 0\text{--}0.1$) hybrid films, which show

an excellent rectification ratio, moderate photoresponse and quantum efficiency under UV illumination.^[54] As the bandgap of Zn_{1–x}Mg_xO films can be tuned between 3.24 and 3.49 eV by varying the value of x , at an reverse bias of 1 V, the maximum responsivity of the devices varies between 0.22 and 0.4 A W^{–1}, and the detectivity varies between 0.17×10^{12} and 2.2×10^{12} Jones.

Um et al. built MoS₂ nanosheet-on-1D CuO nanowire vdW heterojunction PDs with an atomically sharp interface and a high-quality heterojunction. The device structure of these heterojunction PD is displayed in Figure 3g.^[55] The optimized PD exhibits a low dark current of ≈ 38 fA at –2 V (Figure 3h), an ultrahigh responsivity of ≈ 157.6 A W^{–1} under 532 nm laser excitation with intensity of 55 μ W, a high rectification ratio of ≈ 6000 at ± 2 V, and short rise/decay times of $\approx 34.6/51.9$ ms (Figure 3i). Besides, Hong et al. fabricated a self-powered broadband PD by coating an n-silicon nanowire (n-Si NW) array with a layer of p-CuO nanoflakes.^[56] This p–n heterojunction shows excellent

rectification characteristics, a low dark current of 0.7 nA at 0 V and distinctive photovoltaic behavior under broadband light illumination. Under relatively weak visible and near-IR light illumination (0.48 W cm^{-2}), the CuO/Si NW device displays a self-powered high photosensitivity of 1×10^3 and ultrashort rise/recovery times of 60/80 μs . In addition, this PD reveals a distinctive binary response under a small forward bias. It is believed that these superior photoelectric properties are attributed to the specific geometry of the arrayed nanowires, the high surface area, and the built-in field near the CuO/Si NW interface.

3.2.2. Metal Oxide + Organic Semiconductors

p-Type organic materials usually exhibit the advantages of ease of fabricating in large scale, broadband absorption range, and the elastic modulating of their semiconductor characteristics, which make them suitable for photodetection.^[57] The PDs based on the hybridization of p-type organic molecules with tunable functionality and n-type inorganic semiconductors with superior intrinsic carrier mobilities, usually present high photodetecting performance, due to the efficient photoinduced charge transfer and exciton dissociation resulting from the p–n heterojunctions.

Polyaniline (PANI) is a well-known p-type conducting polymer that is suitable for hole collection and transport layer in photoelectronics with p–n junction configuration. Zheng et al. adopted an ordered TiO₂ nanowell thin layer and PANI with various morphologies to construct hybrid self-powered UV PDs.^[58] The hybrid PD with optimized loading amount of PANI exhibits a high responsivity of 3.6 mA W^{-1} , a large on–off ratio of $\approx 10^3$, excellent wavelength selectivity, short response times of 3.8/30.7 ms, and good stability under 320 nm light illumination at 0 V. Moreover, Chen et al. fabricated a high-sensitivity self-powered solar-blind DUV PD based on hybrid organic PANI and inorganic MgZnO bilayer.^[59] At –1 V bias, the optimized PD shows a low dark current of 0.44 pA, a sharp cutoff of responsivity at 271 nm and a high detectivity of 1.5×10^{11} Jones. Owing to the hybrid p–n junction, the PD exhibits a high on/off ratio of 10^4 at 0 V, a responsivity of $160 \mu\text{A W}^{-1}$ at 250 nm, and a high UV–vis (250/400 nm) rejection ratio of up to $\approx 10^4$.

Many other organic materials, such as poly(vinyl alcohol) (PVA),^[60] poly(arcylonitrile) (PAN),^[61,62] poly(vinyl carbazole) (PVK),^[63] polypyrrole (PPy)^[64] and even pyrene tricyanofuran derivatives,^[65] are also adopted to improve the photoelectric properties of metal oxide semiconductor–based PDs. Meng et al. developed a highly ordered 2D TiO₂ nanobowl array/PVK hybrid heterojunction UV PD.^[66] The periodic structure of the 2D TiO₂ NB array contributes to the spectrum selectivity of the devices and emerges the response peak centered at 330 nm. Under 330 nm UV light illumination (144 mW cm^{-2}), the device achieves a high responsivity of 8.14 A W^{-1} at –5 V. The possible transparency, stretchability, flexibility, and ease of production of the organic–inorganic hybrid promote their applications in portable and wearable electronic devices, which are suitable for remote sensing, fiber optic communications and biological imaging.

3.2.3. Metal Oxide + Perovskites

Perovskites with a typical formula of MAPbX₃ (MA = CH₃NH₃; X = Cl, Br, and I), are the representatives of organic–inorganic hybrids. Endowed with unique electrical and optoelectronic properties, perovskites have drawn worldwide researchers' attentions and developed broad applications in light emitting diodes, optically pumped lasers, efficient PEC cells and PDs.^[67] The direct bandgap nature, high absorption ability and complete light absorption of perovskites lead to the high broadband photoresponse of perovskite-based PDs. The short conduction pathways for photogenerated charge carriers lead to fast response speed. Moreover, the very low densities of defects and traps in perovskites ensure the low charge recombination. These characteristics strongly recommend the organic–inorganic hybrid perovskites as ideal building blocks for high-performance PDs. Various perovskites with different structure forms (polycrystalline film, single crystal, and low-dimensional nanostructure)^[68] have been synthesized and combined with metal oxide semiconductors to assemble heterojunction PDs with various device configurations, which demonstrate unprecedented progress in photodetecting performances.

Yi et al. fabricated a TiO₂ nanotube film/CH₃NH₃PbI₃ bilayer device, employing the TiO₂ NT film as a photocarriers transport layer.^[69] The device exhibits satisfactory photoelectric performance with a high on/off ratio of 4000, a high detectivity of 1.85×10^{12} Jones, and short rise/decay times of 0.49/0.56 s. Zheng et al. spin-coated MAPbI₃ quantum dots (QDs) onto the surface of TiO₂ NTs to fabricate TiO₂ NTs/MAPbI₃ QDs heterojunction PDs.^[70] Compared with pure TiO₂ NTs, this heterostructure demonstrates extended response range from UV to visible region, the responsivity in visible range has increased by three orders of magnitude, while its high UV response performance is maintained. This PD demonstrates a relative fast and stable response from 300 to 800 nm and its responsivity reaches to 0.2 A W^{-1} at 700 nm. Apart from the excellent flexibility and high visible-light transparency, the hybrid PD presents good stability to moist air or repeat bending and heating at low temperature.

Similarly, Cao et al. designed and fabricated a hybrid PD consisting of electrospun ZnO nanofibers and perovskites.^[71] Compared to the pristine ZnO or perovskite, the hybrid PD exhibits increased on–off ratio, faster response speed, and higher responsivity and detectivity. The hybrid PDs based on the disordered ZnO nanofibers possess an on/off ratio of 340 and rise/decay times of 0.2/0.7 s. By optimizing ZnO nanofibers to quasialigned arrays, the on/off ratio is further enhanced to 2800, and the rise/decay times change to 0.2/0.5 s. Besides, the responsivity and detectivity reach up to 0.1 A W^{-1} and 10^{13} Jones in the UV and visible regions in correspondence to the band gap of perovskite. Compared with the disordered nanofibers, the quasialigned ZnO nanofiber arrays provide efficient charge transfer between the perovskite and ZnO, shorter transmission paths, and reduced carrier recombination, which contribute to the significantly improved photodetecting performance.

Sun et al. constructed a hybrid PD by combining the n-type InGaZnO thin film and the all-inorganic CsPbBr₃ nanowires together.^[72] This hybrid PD presents excellent photoelectric

properties such as a low dark current of 10^{-10} A at -5 V, a high on–off ratio of 1.2×10^4 , a short response time of 2 ms, and a high responsivity of 3.794 A W^{-1} . It is well acknowledged that the poor chemical stability of perovskite PD in the presence of oxygen and moisture can easily degrade its optoelectronic properties, which hinders its practical application.^[73] However, in this hybrid PD, due to the dual-channel structure of heterojunction, perovskite and IGZO would affect the properties of the heterojunction simultaneously. As a result, the PD shows good stability in ambient for 2 months with little reduction in performance and even exhibits enhanced photocurrent and on–off ratio in high temperature.

3.3. p–i–n Junction

In order to further enhance the performance of p–n junction PD, insulator layer is introduced between p and n layers to form p–i–n structure, which acts not only as the electroblocking layer, but also the light absorption layer to adjust the spectral response range of PD and the spacer layer to prolong the transmission path of electrons in the electric field. It is demonstrated that the hybrid PDs with p–i–n junction structures have several figures of merit such as high breakdown voltage, fast response and low dark current.^[74]

Ling et al. assembled a SnO₂ nanoparticle thin film/SiO₂/p-Si heterojunction PD, which exhibits a stable, repeatable and broadband photoresponse from 365 to 980 nm.^[75] Meanwhile, the optimized PD shows high responsivities of 0.285–0.355 A W^{-1} , an outstanding detectivity of $\approx 2.66 \times 10^{12}$ Jones, an excellent sensitivity of $\approx 1.8 \times 10^6$ cm² W^{-1} , and extremely short response times (<0.1 s). It is believed that the large Fermi energy difference between the SnO₂ nanoparticle thin film and Si lead to a large band offset in the SnO₂/Si heterojunction. With the thin SiO₂ layer as the electroblocking layer and the oxygen vacancy defects in the SnO₂, the carrier transportation in this heterostructure is easily controlled, which facilitates the high-response broadband detection.

3.4. Schottky Junction

Except for the p–n and p–i–n junctions, Schottky junctions formed at the interfaces between conductors (metal or others) and semiconductors are also adopted to construct high-performance PDs, which can detect radiations with photon energies below the bandgap of semiconductors via internal photoemission. Compared with the photoconductive-type PDs, Schottky PDs have numerous advantages, such as fast response speed, low dark current, large UV–vis rejection ratio, and possible self-powering characteristic.^[76] Metals and conductors, such as In, Al, Au, Ni,^[77] Cu–Al–Mn–Ni shape memory alloy, and ITO (indium doped tin oxide), are usually utilized to construct high-performance Schottky photodiodes.

Liu et al. assembled lateral MSM-type UV detectors based on ZnO nanorod with different metal contacts.^[78] With the combined effect from a ZnO seed layer and an inactive layer for nanorod growth, ZnO nanorods could grow laterally and aligned between the interdigitated electrodes. At the end of the

growth process, the integration of ZnO nanorods into a function device can be achieved in the meantime, as presented in **Figure 4a**. The visible–blind devices display great response even in the mid-UV region. It is exhibited in **Figure 4b,c** that the PDs with Ni electrodes show better performance both in the aspects of photocurrent and response time, owing to the larger height of Schottky barrier at the Ni/ZnO interface.

In general, the surface decoration of metal oxide semiconductors by metals NPs can form localized Schottky junctions, which create charge depletion regions at the interface, thereby reducing the dark currents. Moreover, the plasmonic effects, the modification of work functions and the induction of charge transfer caused by the introduction of metals NPs would lead to improved photoelectric performances. Specially, Chen et al. demonstrated the decoration of Au NP at the nanowire surfaces as an effective way to enhance both the photocurrent value and photoconductive gain of a single ZnO NW PD.^[79] The improved photoelectric properties of the Au NP-decorated ZnO NW PD under UV illumination is attributed to the pronounced electron–hole spatial separation effect via the formation of localized Schottky junctions under open-circuit conditions. Besides, the enhanced space charge effect also makes the gain insensitive with the excitation power, which is beneficial for the PD to maintain high gain even with the high-power excitation.

Due to the superior electrical, mechanical, and optical properties of graphene, graphene-based Schottky photodiodes have attracted numerous attentions in recent years. Liang et al. fabricated a graphene/TiO₂ heterojunction PD with high UV light selectivity by simply transferring single-layer graphene on rutile TiO₂ NRs array.^[80] The responsivity and specific detectivity are estimated to be 52.1 A W^{-1} and 4.3×10^{12} Jones, respectively. After the wet-chemistry treatment, the UV PD shows an obviously decreased sensitivity, while the rise/fall times are shorted to 80/160 ms and the specific detectivity is increased to 3.2×10^{13} Jones. Similarly, Nie et al. assembled a monolayer graphene film/ZnO NR array Schottky junction UV PD by coating ZnO nanorod array with a transparent monolayer graphene film. The device structure of this PD is depicted in **Figure 4d**.^[81] This device reveals effective trapping of the incident UV light in the top end of ZnO NR array and exhibits highly stable UV response (**Figure 4e**). A high responsivity of 113 A W^{-1} and a high photoconductive gain of 385 at -1 V is achieved. Meanwhile, the formation of Schottky junction, the high crystallinity of the ZnO NR array and the strong light trapping effect lead to extremely short rise/fall times of 0.7/3.6 ms (**Figure 4f**).

Insulator layer can also be introduced into the MS structure to form metal–insulator–semiconductor (MIS)-structured PD, which can achieve the modulation of photoelectric performance.^[82] Chang et al. fabricated a TiO₂ MIS PD by inserting a polyvinylphenol (PVP) layer in between the metal electrodes and the TiO₂ nanowires.^[83] The PD achieves a 29 times larger photocurrent and an effectively suppressed dark current compared with a TiO₂ nanowire MSM PD. Apart from the stable and reproducible dynamic response with an on/off ratio of around 180, this TiO₂ MIS PD displays a responsivity of 2.46×10^{-3} A W^{-1} under 390 nm at 5 V, a noise equivalent power of 7.49×10^{-12} W and a detectivity of 8.86×10^{11} Jones. This MIS PD also tolerates a higher bias and provides a higher gain to amplify the signal.

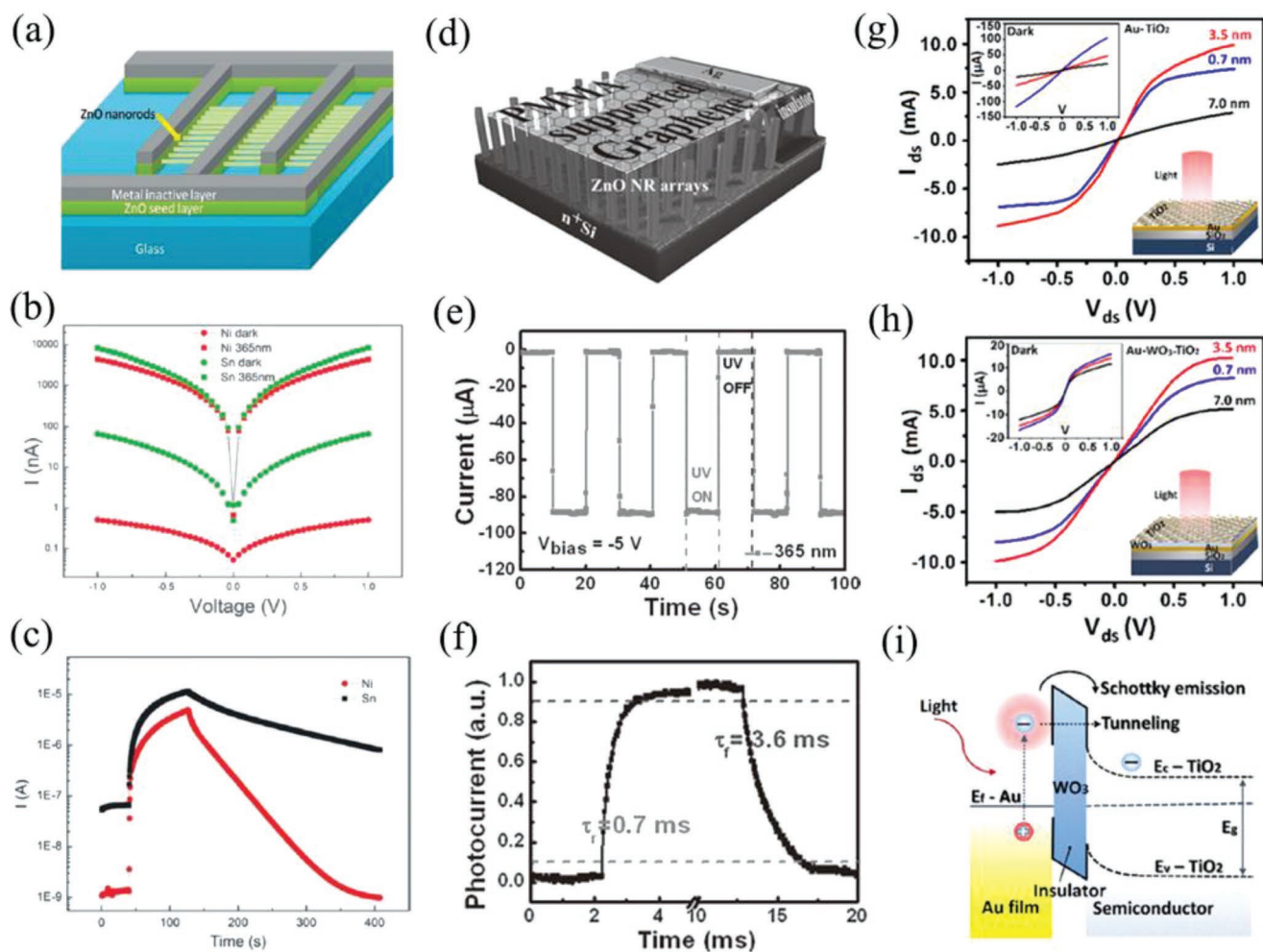


Figure 4. a) Schematic diagram for the UV PD based on laterally aligned ZnO nanorods. b) I - V characteristics of the ZnO nanorod PDs with different metal electrodes measured at 365 nm and in dark. c) UV response-time curves of the ZnO nanorods with Sn and Ni electrodes. d) Schematic illustration of the MLG film/ZnO NR array Schottky junction UV PD. e) I - t curves of the MLG film/ZnO NR UV PD at 365 nm. f) A single normalized I - t cycle at 50 Hz. g, h) I_{ds} versus V_{ds} of the 2D Au-TiO₂ and Au-WO₃-TiO₂ plasmonic devices at 785 nm (power density of 20 mW cm⁻²) with $V_G = 0$ V and $V_{ds} = 1$ V. i) Schematic diagram of the MIS structure with insulator intermediate for the control of the height of Schottky barrier. a-c) Reproduced with permission.^[78] Copyright 2010, American Chemical Society. d-f) Reproduced with permission.^[81] Copyright 2013, Wiley-VCH. g, i) Reproduced with permission.^[84] Copyright 2018, American Chemical Society.

Due to the efficient carrier transport between adjacent layers, 2D heterojunctions are frequently adopted in high-performance PDs. Zhuiykov's group developed 2D Au-TiO₂-based plasmonic devices with 2D MS heterojunctions, which exhibited substantially enhanced photoresponsivity and demonstrated improved response speed under visible light illumination.^[84] To circumvent the undesired dark current in the plasmonic devices, a 2D WO₃ nanofilm (≈ 0.7 nm) was employed as the intermediate layer on the MS interface to develop the MIS 2D heterostructure. As illustrated in Figure 4g,h, the presence of 2D WO₃ between Au and TiO₂ nanofilms results in a slight enhancement of the photocurrent density compared with that of the Au-TiO₂ film. It is also displayed in the insets that the dark current density decreases considerably from 110 μ A of the Au-TiO₂ device to the value of 14 μ A of the Au-WO₃-TiO₂ device at $V_{ds} = 1$ V. As a result, a 13.4% improvement of the external quantum efficiency is obtained for the fabricated 2D Au-WO₃-TiO₂

heterojunctions. The impedancemetry measurements in Figure 4i confirms the modulation of charge transfer at the 2D MS interface using MIS architectures. Besides, broadband photoresponsivities in the UV and visible region are also observed for the Au-WO₃-TiO₂ heterostructures.

3.5. External Applied Field

External applied field such as magnetic field can have great influences on the photoelectric performance of heterojunction PDs.^[85] Deka Boruah and Misra fabricated cobalt-integrated zinc oxide nanorod (Co-ZnO NR) array as a novel heterostructure for UV PD.^[86] This PD exhibits highly tunable photoelastic response, which shows 2.15 times enhancement in response current as compared to the pristine ZnO NRs PD. The applied external magnetic field can enhance the response current

value of this Co–ZnO NRs PD by 186%. It is concluded that the opposite polarizations of electron and holes in the presence of external magnetic field contribute to effective separation of electron–hole pairs that have drifted upon UV illumination. Moreover, the Co–ZnO NRs PD shows much shorter rise/decay times of 1.2/7.4 s, as compared to the 38/195 s of the pristine ZnO NRs. The deeper understanding of the influences of external applied fields on the behaviors of charge carriers in related PDs could provide new pathways to modulate their photoelectric properties.

4. Transportation of the Charge Carriers

4.1. Adjusting Transport Channels

Due to the different nanostructures of metal oxide semiconductors adopted in the PDs, the photogenerated charge carriers can transport towards different dimensions, and the transport channels for the separated charge carriers to go through before they arrive at the electrodes are quite different, thus making a great difference to the photoelectric properties of these PDs.

4.1.1. 0D Structures

0D structures such as nanoparticles and quantum dots have been utilized in metal oxide–based PDs. Jin et al. fabricated a visible–blind solution-processed UV PD based on colloidal ZnO nanoparticles.^[87] The devices exhibit low dark currents with a resistance >1 TΩ, high UV photocurrent efficiencies with a responsivity of 61 A W⁻¹ at 370 nm (1.06 mW cm⁻²) and short rise/decay times of <0.1/≈1 s. Because of the very large surface-to-volume ratio of ZnO NP films, the light-induced desorption of oxygen from the NP surfaces could significantly remove electron traps and increase the free carrier density, which effectively reduces the height of Au/ZnO Schottky barrier for electron injection and contributes to the satisfactory UV photodetection.

Graphdiyne (GD) possesses both sp and sp² carbons with two diacetylenic linkages between the adjacent carbon hexagonal structures and exhibits an electronic conductivity of 2.56 × 10⁻¹ S m⁻¹. It is promising for the optoelectronic and photocatalytic applications for its semiconducting behavior with a theoretical-calculated band gap of 0.47 and 1.12 eV.^[88] Li and co-workers prepared graphdiyne:ZnO nanocomposites by the self-assembly of GD nanoparticles onto the surface of PrA-modified ZnO NPs, and then assembled the nanocomposites into UV PDs.^[89] The junction formed between the GD NP and ZnO NP greatly improves the carrier separation and transport, leading to significantly enhanced photoresponse. The device exhibits a high responsivity of 1260 A W⁻¹ and short rise/decay times of 6.1/2.1 s, compared with a much lower responsivity of 174 A W⁻¹ and much longer rise/decay times of 32.1/28.7 s from the pure ZnO device.

Mitra et al. demonstrated high-performance flexible DUV PDs based on ZnO QDs synthesized by femtosecond-laser ablation in liquid (FLAL) technique.^[90] This method produces highly stable and reproducible ZnO QDs and allows the operation of as-fabricated PDs at ambient conditions. Carbon-doped ZnO QD-based PD can detect efficiently in the DUV spectral

region down to 224 nm. It also exhibits fast response, high photoresponsivity and stability. The 0D characteristic of the ZnO QDs enable the possibility for highly stable flexible devices. Their photoelectric performance could be further improved by exploiting the above-mentioned multiple exciton effect.^[37]

4.1.2. 1D Structures

1D inorganic semiconductor nanostructures, such as nanowires, nanobelts (NBs), nanorods (NRs) and nanotubes, have attracted tremendous research interests as fundamental building blocks for nanoscale electronics and optoelectronics for their unique electrical and optical properties.^[91] 1D nanostructures possess several features that make them candidates for high-performance PDs.^[70] On the one hand, their large surface area to volume ratios cause the existence of numerous trap states at the surface, leading to significantly prolonged lifetime of photogenerated carriers. On the other hand, 1D nanostructures can provide long path length for photon absorption while short channels for carrier transport, leading to increased light absorption and fast carrier transit. Besides, due to their huge aspect ratios, 1D nanostructure is mechanically flexible along their longitudinal direction, which makes it suitable for flexible PDs. The rational design of the morphology and composition of 1D metal oxide nanostructures will enable their utilizations as functional building blocks to build PDs with unique spectral selectivity and sensitivity. Various 1D metal oxide nanostructures including binary oxides (such as ZnO, SnO₂, Ga₂O₃, Nb₂O₅, and WO₃) and ternary oxides (such as Zn₂SnO₄, ZnGa₂O₄, Zn₂GeO₄, and In₂Ge₂O₇) have been successfully synthesized and constructed into PDs.^[92]

Molina-Mendoza et al. deposited individual TiO₂ fibers onto the prepatterned Ti/Au electrodes on SiO₂/Si substrates and characterized their optoelectronic properties.^[93] Figure 5a shows a typical *I*–*V* curve of the PD based on TiO₂ nanofiber in dark and under 455 nm light illumination. The as-fabricated PD presents a high UV responsivity of 90 A W⁻¹ at 375 nm and a short response time of ≈5 s. The PDs are sensitive to light polarization, with an anisotropy ratio of 12%. It is believed that the combination of large surface area and low 1D transport resistance in the electrospun TiO₂ fibers contribute to the fast response and high responsivity. Moreover, Hsu et al. demonstrated a novel strategy to integrate a carbon nanotube and TiO₂ in a core–shell fashion as 1D PD.^[9] Radial Schottky barriers between carbon nanotube cores and TiO₂ shells and surface states at TiO₂ shell surface, facilitate the separation of photogenerated electrons and holes and regulate electron transport, leading to an ultrahigh gain of 1.4 × 10⁴ and ultrashort rise/decay times of 4.3/10.2 ms. Moreover, radial Schottky junction and defect band absorption extend the detection range to visible zone.

Due to the specific 1D nanostructures, the PDs constructed from ZnO single nanowire or nanobelt are expected to exhibit high on/off current ratios and fast response speed. However, the measurement of the very low photocurrent of ZnO single nanowire UV PDs requires high-precision measurement systems, which hinders their further application. Ren et al. prepared ZnO nanowires with unique nanostructure characterized by long chains of closely attached ZnO nanocrystals with ZnO/ZnO nanocrystal

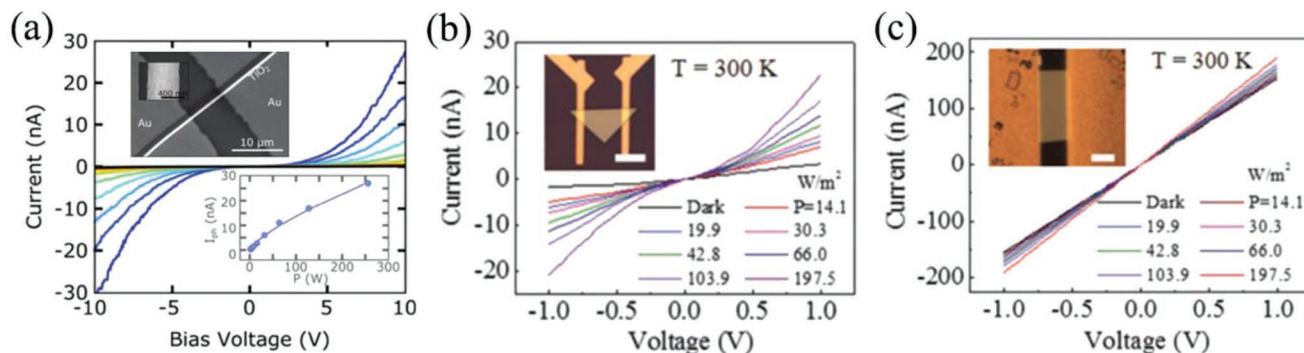


Figure 5. a) Current–voltage characteristics of the TiO₂ nanofiber PD in dark and under 455 nm light illumination. Upper inset: SEM image of a TiO₂ fiber PD. Lower inset: Photocurrent as a function of the light power. b) *I*–*V* curves of a Bi₂O₂Se device under different incident light powers. c) *I*–*V* curves of a Bi₂O₂Se device under different incident light powers. Inset of (b) and (c): Optical images of the devices, the scale bar is 10 μm. a) Reproduced with permission.^[93] Copyright 2016, The Royal Society of Chemistry. b,c) Reproduced with permission.^[99] Copyright 2018, Wiley-VCH.

junctions.^[94] The unique ZnO nanowire-based UV PD exhibits much higher photoresponse currents (at the mA level) and on/off current ratios (≈ 1000) than those of the ZnO nanocrystal-based UV PD. Under the UV irradiance of 120 mW cm⁻² and a low bias of 0.5 V, the peak photocurrent and on/off current ratio of the ZnO nanowire PD are 56 and 36 times higher than those of the ZnO nanocrystal UV PD, respectively.

Wu et al. grew VO₂ microwires on a SiO₂/p-Si(100) substrate and bonded an individual VO₂ microwire onto the ends using silver paste to fabricate a PD.^[95] This VO₂ PD exhibits a linear *I*–*V* curve with a low dark current, while a nonlinear curve is observed by varying the light intensities. The PD achieves an extremely high responsivity of 7069 A W⁻¹, an EQE of $2.4 \times 10^{10}\%$ and a detectivity of 1.5×10^{14} Jones at a bias of 4 V under UV illumination (1 μW cm⁻²). The highly efficient hole-trapping effect resulted from the unequal barrier heights at the two contacts, contribute to the high responsivity and EQE in this VO₂ PD. The responsivity of VO₂ PD is 6 and 4 orders higher than that of the PDs based on graphene (or MoS₂) and GaS, respectively, depicting the great potential of PDs based on metal oxide nanostructures.

Because of their complex functionalities and tunable properties achieved via adjusting the components ratio, 1D ternary oxides show potential applications in photocatalysts, electroluminescence devices, UV PDs, and so forth. Zhou et al. developed high-performance solar-blind DUV PDs based on individual single-crystalline Zn₂GeO₄ nanowires.^[96] The optimized device demonstrates outstanding solar-blind photo-detecting performances with a responsivity of 5.11×10^3 A W⁻¹, an EQE of $2.45 \times 10^6\%$, a detectivity of $\approx 2.91 \times 10^{11}$ Jones, and short rise/decay times of $\approx 10/13$ ms, which shows great advantages over other reported Zn₂GeO₄-based devices.

With respect to the single-crystalline nature of 1D nanostructures adopted in reported PDs, it allows only the band-edge modulation along the radial direction. However, the energy bands are still flat along the axial direction, which inevitably leads to a large dark current due to the intrinsic carrier concentration. He et al. achieved the controlled growth of polycrystalline WO₃ nanobelts via varying the applied voltages in the electrospinning process.^[97] As compared to the single-crystalline counterparts, the polycrystalline NBs present much more crystalline grains and boundaries in the WO₃ NB PD, leading to an effectively suppressed dark currents of 12 pA at

5 V. As a result, this WO₃ NB PD exhibits a high UV sensitivity with an on–off ratio of up to 1000, a spectral responsivity of 2.6×10^5 A W⁻¹ and an ultrahigh EQE of up to $8.1 \times 10^7\%$.

4.1.3. 2D Structure

2D materials possess a layered structure weakly bonded by van der Waals forces in atomic or molecular thickness and infinite planar dimensions, which are easy to prepare and transfer. Varying from zero-gap and semimetallic graphene to broad bandgap semiconductors and large bandgap insulators, 2D materials offer a broad variety of building blocks with remarkable electronic, photonic and mechanical properties and become the research focus in the next few decades.

2D layered semiconductors interact with incident light strongly, presenting satisfactory photon absorption and electron–hole generation. The electronic and optoelectronic properties of 2D layered materials can be easily tuned via adjusting the dimension, conducting intercalation, forming heterostructures, etc., which could lead to improved performance of related devices.^[98] The atomic-thick 2D layered semiconductors with high transparency and good mechanical flexibility provide the possibilities for flexible, wearable, or portable electronics. As an emerging 2D layered material with high carrier mobility, near-ideal sub-threshold swing and high air stability, Bi₂O₂Se has shown great potential for infrared detection. Li et al. prepared high-quality ultrathin Bi₂O₂Se sheets and coexisted Bi₂O_xSe nanosheets via a low-pressure chemical vapor deposition method, and characterized their near-IR photodetection performance.^[99] Figure 5b presents the *I*–*V* curves of the PD based on triangle shaped Bi₂O_xSe nanosheet with different light powers. Compared with the triangle shaped Bi₂O_xSe nanosheet, the PD based on high-quality ultrathin Bi₂O₂Se sheets exhibits more excellent IR detection performance, as shown in Figure 5c. The response time, responsivity and detectivity of the Bi₂O₂Se nanosheets near-IR PD can reach to 2.8 ms, 6.5 A W⁻¹ and 8.3×10^{11} Jones, respectively, showing potentials for ultrafast and flexible PDs.

2D nonlayered materials with both the novel properties of their bulks and the 2D characteristics can be necessary complement to 2D layered materials. For instance, the surfaces of 2D nonlayered materials are filled with the surface dangling

bonds, enabling their surfaces with high chemical activity and enhancing their capability of catalysis, sensing and carriers transfer. 2D nonlayered materials have been developed for optoelectronic devices, including PDs and solar cells.^[100] Sun et al. achieved the molecular self-assembly synthesis of ultrathin 2D nanosheets of transition metal oxides (TiO₂, ZnO, Co₃O₄, and WO₃) by the rational employment of lamellar reverse micelles.^[101] The synthesized ultrathin transition metal oxide nanosheets possess confined thickness, high specific surface area and chemically reactive facets. They were deposited on a single-layer graphene back electrode to build transparent and flexible UV PDs. These PDs exhibit ohmic behaviors, large photocurrent densities up to the order of mA cm⁻² and highly stable and reproducible time response. Hai et al. achieved a WO₃ monolayer with a uniformed thickness of ≈0.74 nm over the large-area Si wafer by atomic layer deposition (ALD).^[102] Under 785 nm light illumination with a power intensity of 2.0 × 10³ mW cm⁻², the as-fabricated monolayer WO₃ PD exhibits a high responsivity of 71.6 A W⁻¹, a high EQE of 1.13 × 10⁴, short response time of ≈2.5–2.7 ms, and superior long-term stability. Their group also grew monolayer WO₃ on large-area SiO₂/Si wafer by ALD.^[103] The deposited WO₃ monolayer exhibits a wider bandgap of 3.53 eV. Under 320 nm UV-A light illumination with a power of 0.25 mW, the monolayer WO₃-based phototransistor-type PDs have demonstrated a photoresponsivity up to ≈0.329 A W⁻¹ at V_{ds} = -5 V, extremely fast response time of less than 40 μs and long-term stability.

Considered the inevitable disadvantages of commonly used wet-chemical methods, it is very important to develop novel and facile methods for the fabrication of high quality 2D nonlayered materials. Feng et al. fabricated 2D polycrystalline Ga₂O₃ nanosheets with a thickness of less than 10 nm from the direct oxidation of GaSe nanosheets.^[104] A solar-blind phototransistor-type PD based on 2D Ga₂O₃ is assembled. Under 254 nm UV light (0.5 mW cm⁻²), the responsivity, detectivity and external quantum efficiency of the PD at V_{ds} = 10 V are 3.3 A W⁻¹, 4.0 × 10¹² Jones and 1600%, respectively. The PD also exhibits fast rise/decay times of 30/60 ms and good stability. As the development of micro/nanofabrication technologies, more metal oxide semiconductor-based 2D nanostructures would be produced and their fascinating properties could facilitate the performance enhancement of related PDs.

4.1.4. Arrays

The application of periodic micro/nanoarrays assembled from 1D and 2D nanostructures, have been extended from highly integrated devices such as FETs and PDs, to flexible PDs, active matrix displays, and PD arrays, which mostly present excellent mechanical, electronic, and optoelectronic properties.^[98] Wu et al. adopted a facile wet-chemical etching approach for controlled patterning of CVD-grown 2D Bi₂O₂Se film and obtained centimeter-scale well-ordered 2D Bi₂O₂Se arrays with tailorable configuration.^[105] The optimized PD assembled from 2D Bi₂O₂Se arrays displays a negligible dark current of ≈3 nA at V_{ds} = 0.1 V, a high photoresponsivity of ≈2000 A W⁻¹ at 532 nm with the incident power of ≈0.1 nW and excellent air stability. Goswami et al. synthesized 1D perpendicular In_{2-x}O_{3-y} nanostructure arrays with highly porous structure

by using the glancing angle deposition (GLAD) technique.^[106] The 1D In_{2-x}O_{3-y} based PD exhibits a maximum responsivity of ≈15 A W⁻¹ and an internal gain of ≈47 at ≈380 nm, which corresponds to the near band gap transition of the In₂O₃ columnar array. Compared to the In₂O₃ NP and In₂O₃ nanorod based PDs, the vertical transportation of the photoinduced carriers in the nanostructure arrays through the short distance towards electrodes facilitates the shortening of rise/decay times to 1.9/2.3 s.

4.1.5. Composite Films

The weak photon absorption and high recombination rate of electron-hole pairs in individual metal oxide nanostructures limit their applications in photodetection. Composite films constructed by mix-dimensional nanostructures can take advantages of the specific properties of different components, so as to achieve the synergic improvements of photoelectric properties.^[107]

Carbon materials such as graphene, graphdiyne, activated carbon and carbon nanotubes, are suitable candidates for composite film PDs owing to their superior optical and electric properties.^[108,109] Chen et al. proposed the UV-assisted photochemical reduction of GO in zinc oxide nanowires (ZNWs) suspension to achieve the formation of graphene sheets attached in ZNWs network and the enhancement of UV absorption.^[110] Compared with the PDs based on pure ZNWs, the optimized PD based on RGO/ZNWs composite exhibits an enhanced photoresponse with a photocurrent density of 5.87 mA cm⁻², an on/off current ratio of 3.01 × 10⁴, and a responsivity of 1.83 A W⁻¹ under a UV irradiation (3.26 mW·cm⁻²) at 1.0 V. It is deduced that the extremely large interface area of graphene/ZNWs suppresses the carrier recombination and improves the carrier transport, thus leading to the photoresponse enhancement. Saravanan et al. prepared granular activated carbon (GAC) materials via the simple gas activation of silkworm cocoons and coated them on the ZnO nanorods (ZNRs) to form a core-shell structure.^[111] Compared to the low photocurrent (≈1 μA) of the PD based on ZnO NPs in **Figure 6a,b**, the as-assembled GAC/ZNR core-shell UV PD exhibits a superior photocurrent of 16 mA in **Figure 6c,d**. As the well-aligned GAC/ZNR core-shell structure exhibits strong light absorption and increased generation of charge carriers, the GAC/ZNR PD exhibits a high on-off ratio of 1585, compared to the low on-off ratio of 40 from the as-grown ZNR PD. Apart from the fast adsorption ability of GAC, the finest distribution of GAC on ZNRs results in rapid electron transportation between the conduction bands of GAC and ZNRs, leading to shortened rise/decay times. Furthermore, this core-shell structure-based UV PD also exhibits good repeatability and long-term stability.

Plasmonic metal NPs and dyes are also utilized to modify the light absorption of composite film, so as to achieved enhanced performance. Wang et al. demonstrated Ag NP-decorated ZnO PDs for UV light sensing.^[112] Due to the localized Schottky junction between ZnO film and Ag NPs, the dark current density of ZnO UV PDs decreases obviously from 60 to 38 mA cm⁻². In particular, the device exhibits obviously increased peak responsivity at around 380 nm, which can be attributed to the strong incident light scattering derived from the narrow-band quadrupole plasmon resonance of Ag NPs in the UV range.

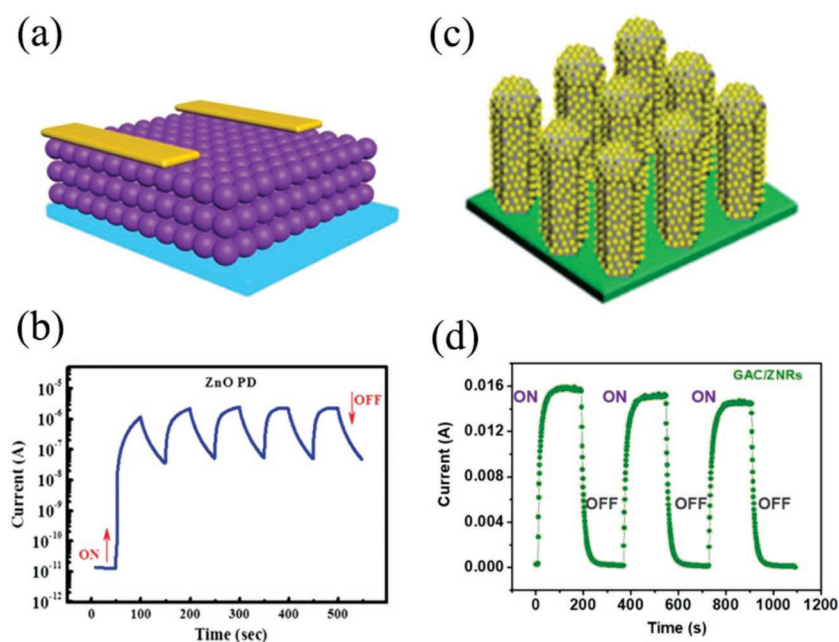


Figure 6. a) Schematic illustration of the fabricated PDs based on the ZnO film. b) On–off switching properties of the corresponding ZnO PD. c) Schematic illustration of the ZNR@GAC core–shell structure. d) On–off switching properties of the corresponding ZNR@GAC PD. a,b) Reproduced with permission.^[89] Copyright 2016, Wiley-VCH. c,d) Reproduced with permission.^[111] Copyright 2017, American Chemical Society.

Besides, the shading effect and surface defect passivation of Ag NPs cause the dramatic decreases of responsivities at the other wavelengths. As a result, the response peak at around 380 nm becomes more significant and the response of device presents excellent wavelength selectivity. Mottram et al. developed dye-sensitized thin-film phototransistors consisting of ultrathin In_2O_3 layers (<10 nm) and self-assembled monolayers of light absorbing organic dye D102.^[113] In accompany with the extremely high internal signal gain resulted from the improved electronic coupling in this unique heterostructure, the optimized transistor exhibits a preferential photoresponse centered at ≈ 500 nm with a maximum photosensitivity of $\approx 10^6$ and a responsivity of up to $2 \times 10^3 \text{ A W}^{-1}$. Moreover, the hybrid $\text{In}_2\text{O}_3/\text{D102}$ bilayer channel appears transparent with an average optical transmission of >92% in the wavelength range of 400–700 nm, depicting its great potentials for transparent PDs.

4.2. Other Factors Influencing the Carrier Transport

Except for the heterojunctions, there are some other factors such as crystallinity of semiconductors, applied bias voltage and surface/interface problems, having influences on the behavior of carriers in the transport process. Corresponding measures have been taken to deal with these factors.

4.2.1. Improved Crystallinity

The photoelectric properties of semiconductors are strongly affected by their crystallinities, which are dominated by the

preparation process and post-treatments. The excess defects and grain boundaries of the building blocks in the semiconductor crystals would increase the trapping and recombination possibilities of photogenerated charge carries on their way towards electrodes, thus leading to weakened photoresponse. To minimize this deficiency, it is necessary to adopt exquisite and precise preparation processes as well as appropriate post-treatments to fabricate semiconductor crystals with high crystallinity and moderate defects, so as to increase the efficiency of charge-carrier transport and improve the photoelectric performance of related PDs.

4.2.2. Applied Bias Voltage

The applied bias can accelerate the diffusion of charge carriers toward electrodes along the direction of electric field. Forced by the applied bias, the depletion of the charge carriers out of the junctions is reduced, which leads to increased photocurrent and shortened response times. However, the further increase of applied voltage will increase the short noise and lead to increased dark current and power consumption.^[114] Thus, it is necessary to choose an appropriate operation voltage to make a balance between high performance and facile power supply in practical application.

4.2.3. Surface/Interface Carrier-Transport Modulation

As for the optoelectronic devices constructed from nanostructures, the dramatically increased surface-to-volume ratios, interfacial areas and surface–environment interactions have great influences on the device performance. The modulation of surface/interface charge-carrier generation, diffusion, and recombination/transport processes should be taken into considerations in constructing high-performance PDs. For metal oxide nanomaterials, the presence of abundant deep-level states at the surfaces of metal oxides combining with a gas desorption/reabsorption process could contribute to high photosensitivities.^[115] The surface effects resulted from engineering the size of nanomaterials and several surface treatments, such as heat treatments and Au–NP decoration, have demonstrated impacts on the surface band bending, which dominates the photon–electron conversion behaviors. By modifying the specific thin depletion region near the surface, the optoelectronic properties of PDs based on metal oxides nanostructures are tunable.^[116,117] However, due to the slow photo-carrier relaxation behaviors caused by the surface adsorption/desorption processes, a long recovery time has been observed in PDs based on single metal oxide nanostructure. To achieve both increased photosensitivities and shortened recovery time, several strategies including the introduction of heterojunctions and the construction of core–shell and network geometries to

achieve the modulation of interface carrier transport have been proposed.^[9,19,118] Chen et al. grew ZnO nanobelt networks on the prefabricated Ti/Au electrodes by a vapor-liquid-solid method and fabricated the ZnO NB-network PD.^[119] Compared with a long recovery time of 32.95 s in the single ZnO NB-based PD, a fast recovery time of 0.53 s is observed in the ZnO NB-network PDs. The significantly shortened recovery time resulted from the dominated electron transport, which is achieved by a number of NW–NW junction barriers formed in the network.

To go a step further, by taking advantages of photon-trapping, surface plasmonic resonance (SPR), piezophototronic effects, and interface carrier-trapping/transport control, Guo et al. designed a photon-alternative UV PD based on self-bending-assembled ZnO nanowires.^[120] The carriers could be efficiently controlled by the surface/interface states of these ZnO nanowires. Through effective surface/interface carrier-transport modulation, detectivities as high as $1.69 \times 10^{16}/1.71 \times 10^{16}$ Jones at 380 nm with 0.2 V bias are realized by alternating nanoparticle/nanowire active layers, respectively. Meanwhile, the optimized UV PD shows short rise/decay times of 0.023/4.79 ms, which could satisfy the practical needs. The detailed explorations of carrier generation, diffusion, and recombination/transport processes are beneficial to figure out the charge-carrier dynamics contributing to the photoresponse behavior and to come up with corresponding measures to improve the photoelectric performance of metal oxide semiconductor-based PDs.

5. Collection of the Charge Carriers

5.1. Contact Type

Most of the key performance parameters of electronic and optoelectronic devices, such as photocurrent, on/off ratio and response speed, are significantly affected by the electrical contacts connecting the channel with external circuits.^[121] The macroscopic contact resistance is determined by the Schottky barrier height defined by the band alignment between the semiconductor channels and metal electrodes, the doping degree of the semiconductor, and the quality of interface. The device configuration of PDs has great effects on the contact resistance, which is crucial for their performance parameters. With low contact resistances, the PDs with Ohmic contact normally possess excellent properties including large photoconductive gain and high responsivity. The ohmic contact can be realized through combining a contact metal with a matched work function with the band structure of the channel material. After the exclusion of the Fermi level–pinning effect which results in almost unchanged Schottky barrier height, various strategies including changing the contact metal (such as Au, Cr, Ti, Pd, Ni, and even graphene), heavily doping by ion implantation and edge contacts, have been proposed to achieve ohmic contact and improved device performance.

5.2. Electrode Configuration

Metals with large work functions would form Ohmic contacts with p-type semiconductors, while metals with low work

functions would form Schottky junctions with p-type semiconductors. Excluding the influences from the surface states of semiconductors, the adoption of two metal electrodes with large difference in work functions causes asymmetric metal contacts and a built-in potential, endowing Schottky diodes with rectifying and self-powering characteristics. Ouyang et al. grew bismuth oxychloride (BiOCl) nanosheet arrays on a piece of Cu foil (denoted as BiOCl–Cu) and fabricated the BiOCl–Cu samples into BiOCl–Cu-1 and BiOCl–Cu-2 PDs by adopting different electrode configurations.^[114] Under 350 nm light illumination at 5 V, the BiOCl–Cu-1 PD with both Ag electrodes on the BiOCl film yields a relatively high photocurrent of 353 pA, the rise/decay times are calculated to be 0.56/0.59 s. Moreover, a higher photocurrent of 1040 pA is achieved by the BiOCl–Cu-2 PD with one Ag electrode on the BiOCl film and the Cu foil substrate as the other electrode, while the response speed remains nearly the same. Due to the different work functions of the Cu foil and the Ag electrodes, a self-powering characteristic is also presented in this PD. At 0 V bias, the BiOCl–Cu-2 PD achieves a photocurrent of 11.81 pA at 350 nm with an on–off ratio of 125.3.

The design of the Schottky barriers with asymmetric electrode shapes on the PDs can achieve photodetection with a low or even zero power supply. Chen et al. demonstrated a novel ZnO PD based on the asymmetric MSM structure consisting of one Au interdigitated electrode with wide fingers and the other one with narrow fingers.^[122] These ZnO PDs exhibit attractive self-powered characteristics, the increase of asymmetric ratio between the width of wide fingers and narrow fingers in the interdigitated electrodes leads to the enhanced responsivity of this ZnO self-powered UV PD, which reaches up to 20 mA W^{-1} for an asymmetric ratio of 20:1. A physical model based on band energy theory has been developed to illustrate the origin of the photoresponse at 0 V in this device, which demonstrates a new route to assembling self-powered PDs. By using a 2D physical model based on the drift-diffusion theory, Song et al. investigated the influences of asymmetric semicircular and asymmetric triangular Schottky barriers on the photoelectric performance of MgZnO MSM PD.^[123] At 5 V, compared to the MgZnO MSM PD with symmetric rectangular Schottky barrier, the dark currents of the MgZnO MSM PDs with asymmetric semicircular and triangular Schottky barrier are reduced by a factor of 15 for each electrode structure, while the photocurrents are enhanced by factors of 1.2 and 2, respectively. The highest on/off ratio of 7294 is achieved in the MgZnO MSM PD with asymmetric triangular Schottky barrier at a bias of 5 V under 260 nm light illumination with a power of $0.4 \mu\text{W}$. By incorporating different metals to provide a higher asymmetry, the on/off ratio of these PDs can be further increased.

If the time for the charge carrier to travel between two electrodes is shorter than the life time of charge carriers, the charge carrier could transfer through the channel for several times before their combination, leading to enhanced responsivity and gain while prolonged response time.^[124] Miao et al. fabricated black phosphorus (BP) Schottky diodes with asymmetric metal contacts between gold and aluminum electrodes.^[125] The work function difference between the two metal electrodes results in a built-in potential, endowing BP Schottky diodes with rectifying characteristics. With a relatively long channel length of $\approx 1 \mu\text{m}$,

the BP Schottky diode exhibits rectifying behavior with a rectification ratio of 1.05×10^2 at a gate voltage of 0 V. Under 650 nm light illumination with an intensity of 38 W cm^{-2} , the responsivity and EQE measured at $V_{ds} = -1 \text{ V}$ and $V_{GS} = 10 \text{ V}$ are calculated to be $\approx 3.5 \text{ mA W}^{-1}$ and 0.65%, respectively. Besides, the BP Schottky diode exhibits fast response, the rise time and fall time are both less than 2 ms. At an ultrashort channel length of $\approx 30 \text{ nm}$, the device exhibits a current rectification ratio ($I_{forward}/I_{reverse}$) of up to 1.5×10^3 at the gate voltage of -20 V . However, the electric field-induced barrier thinning causes significantly increased tunneling current under reverse bias, leading to nonrectifying output characteristics. In view of these related references, it is necessary to adopt suitable channel length to balance the photoresponse and response speed.

6. Conclusion and Prospective

Varied strategies that researchers have utilized to improve the photoelectric performance of metal oxide semiconductor-based PDs have been reviewed and summarized, in accordance with the different steps those photoinduced charge carriers have involved in the photoelectric conversion process. The charge-carrier engineering has proved its effectiveness on achieving enhanced photoresponse and improved response speed of these PDs. An ideal PD should meet different requirements in terms of excellent spectral selectivity, high responsivity, large detectivity, fast speed, and excellent stability. Until now, there are substantial technological issues remaining in improving the photoelectric properties of PDs based on metal oxide semiconductors. Since most of the as-developed strategies only achieve performance enhancement from one single aspect without systematic consideration, it is urgent to conduct the exploration of novel sensitive semiconductor nanostructures and the efficient engineering of device architecture simultaneously. More efforts should be devoted to deepening the understanding of how the behaviors of charge carrier influence the photoelectric performance of the related PDs and exploring more systematic strategies to improve the efficiency of photoelectric conversion process.

In recent years, numerous new trends and requirements, such as broadband photodetection, self-powering characteristic, adoption of 2D vdW heterostructures, and performance enhancement achieved by specific effects in developing high-performance PDs based on metal oxide semiconductors, have been revealed.

1) *Broadband Photodetector*: PDs with a broad spectral response from the ultraviolet, visible to the near infrared region have attracted fast-growing interests in a variety of applications, including image sensing, chemical/biological sensing, optical communication, daylong surveillance, etc. Unfortunately, the wide bandgap nature of most metal oxide semiconductors determines that they are only suitable for UV-vis PD because of the light absorption limited in the UV-vis region. Thus, combining oxide semiconductors with narrow bandgap semiconductors such as metal sulfides to extend their absorption range into NIR region is crucial for the construction of broadband PDs.^[126] Li et al. developed hybrid nanostructures

of SnS quantum dots and Zn_2SnO_4 nanowires as light sensors.^[127] Compared with the pristine Zn_2SnO_4 nanowire PD, the hybrid PD exhibits high photoconductive gain of up to 1.6×10^6 and specific detectivity of up to 3.8×10^{16} Jones in the UV region. Meanwhile, the photoresponse range extends from the UV to the NIR region. This PD still displays a responsivity up to 19 A W^{-1} at 950 nm, which corresponds to the bandgap of SnS ($\approx 1.3 \text{ eV}$). Besides, taking advantages of some specific effect can also endow semiconductor systems with the ability of broadband photodetection. It is interesting to consider the coupling between new structural concepts and optoelectronic applications based on up (down) converters,^[128,129] which can achieve light harvesting in the long (short) spectral range and the extended photon up(down)-conversion range using sunlight irradiation and optimized device configuration for maximum energy conversion.

2) *2D van der Waals Heterostructures*: The high mobility, 2D, and thickness-dependent bandgap and light absorption endow 2D materials with favorable optical properties and electronic performances, which have attracted tremendous interests in many fields including FETs, solar cells, PDs, and flexible electronics.^[130] 2D vdW heterostructures with smooth heterointerface, tunable bandgap, and ultrafast carrier transport are advantageous for applications in high-performance PDs. Their atomically thin thickness results in ultrafast charge transfer confined in 2D, and the strong light-matter interactions lead to enhanced light absorption, contributing to the fast response speed, large responsivity, and high sensitivity of PDs. By choosing appropriate materials and stacking sequences with careful band alignment engineering, high-performance optoelectronic devices based on 2D vdW heterostructures such as SnO/MoS_2 ^[131] and MoS_2/VO_2 ^[132] have been fabricated.^[133] Chen et al. built hybrid n-type 2D-layered MoSe_2 /p-type MoO_x vdW heterojunction PDs on SiO_2/Si substrates.^[134] These vertical MoSe_2 - MoO_x p-n heterojunction PDs display obvious rectifying characteristics. The optimized device exhibits a responsivity of 3.4 A W^{-1} , a detectivity of 8.5×10^7 Jones, and an EQE of 1665.6% at V_{ds} of 5 V under 254 nm light illumination (0.29 mW cm^{-2}). Besides, the flexibility and transparency of the vdW structure endow this PD great potentials for wearable optoelectronics.

3) *Self-Powered Photodetectors*: The self-powered PDs, which can operate with low power consumption or without any external power supply, have attracted considerable attention for the next-generation optoelectronic devices.^[135] By exploiting the photovoltaic effect or utilizing the built-in energy harvesting unit to convert the incident light into an electrical signal, self-powered PDs can achieve the independent, sustainable, and maintenance-free monitoring of ambient light, which are promising for portable/wearable electronics and working in harsh conditions. Self-powered PDs can be generally classified into two different types. One contains photoconductive devices integrated with energy harvesting units such as nanogenerators, solar cells, and supercapacitors, which can collect energy from the external environment and drive the light sensor to achieve detection.^[136] The other one is photovoltaic PD based on the photovoltaic effect. According to the charge separation features of different interfaces, they can be divided into three types: Schottky junction, p-n/n-n junction, and

PEC cell.^[137,138] Zhao et al. constructed a self-powered solar-blind PD based on a highly crystallized ZnO–Ga₂O₃ core-shell heterostructure microwire.^[139] At zero bias, the PD displays an ultrahigh responsivity of 9.7 mA W⁻¹ at 251 nm and a fast response speed (rise/decay times of <100/900 μs), which make it highly suitable for self-powered photodetection in practice. The deeper insight into the relationship of photoresponse properties with material structure and device configuration is required to construct high-performance self-powered PD.^[44] Moreover, the piezophototronic effect,^[140] thermophototronic effect,^[141] photogating effect,^[142] as well as the coupling between ferromagnetic electrodes and nanostructured materials^[143] are novel routes to improving the self-powering performance of PDs.

4) *New Concept Photodetectors*: Remarkable features such as transparency,^[144] flexibility,^[145] stretchability,^[146] printability,^[147] and multifunctionality^[148] are in great need for the construction of novel wearable,^[149] visualized,^[150] wireless, and real-time^[151] PDs. These emerging new-concept PDs would benefit daily life and industrial production greatly.^[152] By using printable ZnO nanowires and carbon electrodes with origami-based techniques, Lin et al. fabricated a simple and low-cost paper-based PD array featuring

superior deformability.^[118] This device presents an on-off ratio of 13.4 and a detectivity value of 8.14×10^8 Jones under UV illumination (3.8 mW cm^{-2}) at 10 V bias. It also demonstrates reliable detection of UV light at a wide range of intensities. With a folded Miura structure, the paper PD array can be oriented in four different directions via tessellated parallelograms to endow the device with excellent omnidirectional light-harvesting capabilities. Moreover, benefiting from this paper folding technique, the device can be repeatedly stretched (up to 1000% strain), bent (bending angle $\pm 30^\circ$), and twisted (up to 360°) without noticeable performance degradation. This highly deformable electronics design featuring the Miura origami structure provides guidances for the future developments of flexible and deformable PDs. Specially, our group developed a fiber-shaped p-CuZnS/n-TiO₂ UV PD, as presented in **Figure 7a**. Benefiting from the unique nanotube array structure and p–n junction, this PD exhibits an outstanding responsivity of 640 A W⁻¹, a high EQE of $2.3 \times 10^5\%$, and a large photocurrent value of $\approx 4 \text{ mA}$ at 3 V under 350 nm UV illumination (1.26 mW cm^{-2}), as shown in Figure 7b,c.^[153] Meanwhile, it shows a self-powered property with a high responsivity of 2.5 mA W⁻¹ and a short response time of less than

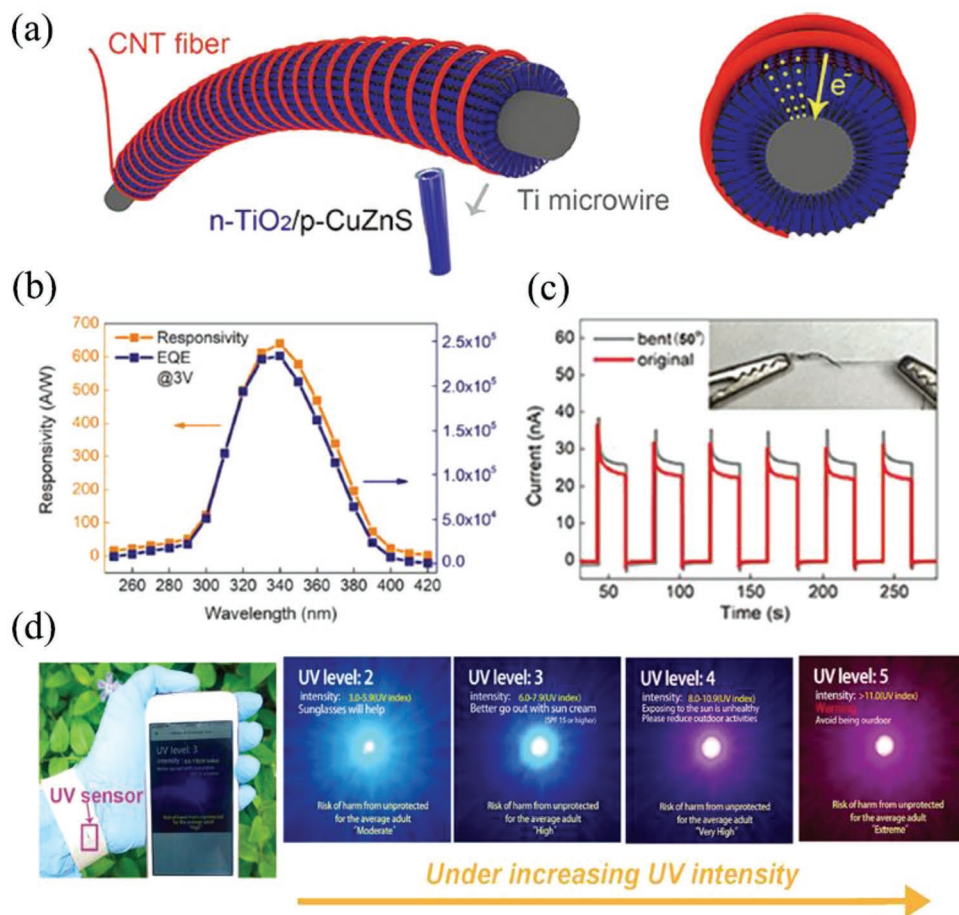


Figure 7. a) Device structure of the fiber-shaped p-CuZnS/n-TiO₂ NTAs PD. b) Responsivity and EQE of the fiber-shaped UV PD as a function of wavelength at 3 V. c) The on-off switching tests of the fiber-shaped PD at the straight state and bent state ($\approx 50^\circ$). d) Schematic illustration of the wearable PD as a real-time UV monitor. Reproduced with permission.^[153] Copyright 2018, WILEY-VCH.

0.2 s at 0 V under 300 nm UV illumination (0.48 mW cm^{-2}). The ultrahigh photocurrent enables it to be easily integrated with commercial electronics to function as a real-time monitor system. Thus, the first real-time wearable UV radiation sensor that reads out ambient UV power density and transmits data to smart phones via wireless network is demonstrated (Figure 7d). This work not only presents a promising wearable health monitor, but also provides a general strategy for designing and fabricating smart wearable electronic devices.

To promote the practical applications of metal oxide semiconductor-based PDs, much more attention should be paid to achieve low-cost and large-scale preparation of sensitive metal oxide semiconductor materials and fabrication of high-performance PDs. Several preparation methods such as anodization, chemical bath, and spray pyrolysis are suitable for large-scale production of metal oxide nanostructures. The adoption of facile, convenient, and cost-effective assembly technologies such as printable electronics technology and laser direct writing method can achieve the fabrication of photoelectric devices in large scale and reduce the cost efficiently. Subsequently, the convenience provided by the PDs based on metal oxide semiconductor nanostructures can be expected and enjoyed in the near future.

Acknowledgements

W.X.O. and F.T. contributed equally to this work. The authors acknowledge the support from the National Key R&D Program of China (Grant No. 2017YFA0204600), the National Natural Science Foundation of China (Grant Nos. 51721002, 51872050, 11674061, and 11811530065), the China Postdoctoral Science Foundation (Grant No. 2018M640338), and Science and Technology Commission of Shanghai Municipality (Grant Nos. 18520744600, 18520710800, and 17520742400).

Conflict of Interest

The authors declare no conflict of interest.

Keywords

charge-carrier engineering, heterojunctions, metal oxide semiconductors, photodetectors, photoelectric performance

Received: October 31, 2018

Revised: December 16, 2018

Published online: January 18, 2019

- [1] H. Y. Chen, H. Liu, Z. Zhang, K. Hu, X. S. Fang, *Adv. Mater.* **2016**, *28*, 403.
- [2] C. Bao, J. Yang, S. Bai, W. Xu, Z. Yan, Q. Xu, J. Liu, W. Zhang, F. Gao, *Adv. Mater.* **2018**, *30*, 1803422.
- [3] T. Okino, S. Yamahira, S. Yamada, Y. Hirose, A. Odagawa, Y. Kato, T. Tanaka, *Sensors* **2018**, *18*, 314.
- [4] K. Liu, M. Sakurai, M. Aono, *Sensors* **2010**, *10*, 8604.
- [5] T. Zhai, X. S. Fang, M. Liao, X. Xu, H. Zeng, B. Yoshio, D. Golberg, *Sensors* **2009**, *9*, 6504.
- [6] L. X. Zheng, K. Hu, F. Teng, X. S. Fang, *Small* **2017**, *13*, 1602448.
- [7] X. S. Fang, L. F. Hu, K. F. Huo, B. Gao, L. J. Zhao, M. Y. Liao, P. K. Chu, Y. Bando, D. Golberg, *Adv. Funct. Mater.* **2011**, *21*, 3907.
- [8] M. Li, J. Zhang, H. Gao, F. Li, S. E. Lindquist, N. Wu, R. Wang, *ACS Appl. Mater. Interfaces* **2016**, *8*, 6662.
- [9] C.-Y. Hsu, D.-H. Lien, S.-Y. Lu, C.-Y. Chen, C.-F. Kang, Y.-L. Chueh, W.-K. Hsu, J.-H. He, *ACS Nano* **2012**, *6*, 6687.
- [10] L. Sang, M. Liao, M. Sumiya, *Sensors* **2013**, *13*, 10482.
- [11] F. Wang, S. Bai, W. Tress, A. Hagfeldt, F. Gao, *npj Flexible Electron.* **2018**, *2*, 22.
- [12] S. Baia, N. Zhang, C. Gao, Y. Xiong, *Nano Energy* **2018**, *53*, 296.
- [13] D. Sett, S. Sanjit, D. Basak, *RSC Adv.* **2014**, *4*, 58553.
- [14] S. Mondal, D. Basak, *Appl. Surf. Sci.* **2018**, *427*, 814.
- [15] J. Jiang, C. Ling, T. Xu, W. Wang, X. Niu, A. Zafar, Z. Yan, X. Wang, Y. You, L. Sun, J. Lu, J. Wang, Z. Ni, *Adv. Mater.* **2018**, *30*, 1804332.
- [16] H.-P. Wang, J.-H. He, *Adv. Energy Mater.* **2017**, *7*, 1602385.
- [17] H.-P. Wang, A.-C. Li, T.-Y. Lin, J.-H. He, *Nano Energy* **2016**, *23*, 1.
- [18] H.-P. Wang, D.-H. Lien, M.-L. Tsai, C.-A. Lin, H.-C. Chang, K.-Y. Lai, J.-H. He, *J. Mater. Chem. C* **2014**, *2*, 3144.
- [19] D.-H. Lien, H.-P. Wang, S.-B. Chen, Y.-C. Chi, C.-L. Wu, G.-R. Lin, Y.-C. Liao, J.-H. He, *npj Flexible Electron.* **2018**, *2*, 19.
- [20] M. X. Hu, F. Teng, H. Chen, M. Jiang, Y. Gu, H. Lu, L. Hu, X. S. Fang, *Adv. Funct. Mater.* **2017**, *27*, 1704477.
- [21] M. Dutta, T. Ghosh, D. Basak, *J. Electron. Mater.* **2009**, *38*, 2335.
- [22] S.-J. Young, Y.-H. Liu, *IEEE Trans. Electron Devices* **2016**, *63*, 3160.
- [23] R. Shabannia, *Mater. Lett.* **2018**, *214*, 254.
- [24] C.-L. Hsu, S.-J. Chang, *Small* **2014**, *10*, 4562.
- [25] R. Jiang, B. Li, C. Fang, J. Wang, *Adv. Mater.* **2014**, *26*, 5274.
- [26] X. Li, J. Zhu, B. Wei, *Chem. Soc. Rev.* **2016**, *45*, 3145.
- [27] J.-A. Huang, L.-B. Luo, *Adv. Opt. Mater.* **2018**, *6*, 1701282.
- [28] Q. Cui, Y. Yang, J. Li, F. Teng, X. Wang, *Crystals* **2017**, *7*, 149.
- [29] K. Hu, H. Chen, M. Jiang, F. Teng, L. Zheng, X. S. Fang, *Adv. Funct. Mater.* **2016**, *26*, 6641.
- [30] C. Tian, D. Jiang, B. Li, J. Lin, Y. Zhao, W. Yuan, J. Zhao, Q. Liang, S. Gao, J. Hou, J. Qin, *ACS Appl. Mater. Interfaces* **2014**, *6*, 2162.
- [31] Z. Guo, D. Jiang, N. Hu, X. Yang, W. Zhang, Y. Duan, S. Gao, Q. Liang, T. Zheng, J. Lv, *Nanoscale Res. Lett.* **2018**, *13*, 168.
- [32] F. Barati, M. Grossnickle, S. Su, R. K. Lake, V. Aji, N. M. Gabor, *Nat. Nanotechnol.* **2017**, *12*, 1134.
- [33] A. V. Zayats, S. Maier, *Adv. Opt. Mater.* **2017**, *5*, 1700508.
- [34] W. X. Ouyang, F. Teng, M. Jiang, X. S. Fang, *Small* **2017**, *13*, 1702177.
- [35] A. Pescaglini, A. Martin, D. Cammi, G. Juska, C. Ronning, E. Pelucchi, D. Iacopino, *Nano Lett.* **2014**, *14*, 6202.
- [36] H. Shokri Kojori, J. H. Yun, Y. Paik, J. Kim, W. A. Anderson, S. J. Kim, *Nano Lett.* **2016**, *16*, 250.
- [37] A. J. Nozik, *Nat. Nanotechnol.* **2009**, *4*, 548.
- [38] O. E. Semonin, J. M. Luther, S. Choi, H.-Y. Chen, J. Gao, A. J. Nozik, M. C. Beard, *Science* **2011**, *334*, 1530.
- [39] R. D. Schaller, V. M. Agranovich, V. I. Klimov, *Nat. Phys.* **2005**, *1*, 189.
- [40] L. Li, L. Gu, Z. Lou, Z. Fan, G. Shen, *ACS Nano* **2017**, *11*, 4067.
- [41] S. Lei, F. Wen, L. Ge, S. Najmaei, A. George, Y. Gong, W. Gao, Z. Jin, B. Li, J. Lou, J. Kono, R. Vajtai, P. Ajayan, N. J. Halas, *Nano Lett.* **2015**, *15*, 3048.
- [42] X. Chen, Y. Xu, D. Zhou, S. Yang, F.-f. Ren, H. Lu, K. Tang, S. Gu, R. Zhang, Y. Zheng, J. Ye, *ACS Appl. Mater. Interfaces* **2017**, *9*, 36997.
- [43] B. Zhao, F. Wang, H. Chen, Y. Wang, M. Jiang, X. S. Fang, D. Zhao, *Nano Lett.* **2015**, *15*, 3988.
- [44] W. Tian, Y. Wang, L. Chen, L. Li, *Small* **2017**, *13*, 1701848.
- [45] W. X. Ouyang, F. Teng, X. S. Fang, *Adv. Funct. Mater.* **2018**, *28*, 1701778.
- [46] C.-L. Hsu, Y.-D. Gao, Y.-S. Chen, T.-J. Hsueh, *ACS Appl. Mater. Interfaces* **2014**, *6*, 4277.
- [47] P.-J. Li, Z.-M. Liao, X.-Z. Zhang, X.-J. Zhang, H.-C. Zhu, J.-Y. Gao, K. L. Laurent, Y. L. Wang, N. W. Wang, D.-P. Yu, *Nano Lett.* **2009**, *9*, 2513.

- [48] P. K. Vabbina, R. Sinha, A. Ahmadivand, M. Karabiyik, B. Gerislioglu, O. Awadallah, N. Pala, *ACS Appl. Mater. Interfaces* **2017**, *9*, 19791.
- [49] T. H. Flemban, M. A. Haque, I. Ajia, N. Alwadai, S. Mitra, T. Wu, I. S. Roqan, *ACS Appl. Mater. Interfaces* **2017**, *9*, 37120.
- [50] Y. T. Lee, P. J. Jeon, J. H. Han, J. Ahn, H. S. Lee, J. Y. Lim, W. K. Choi, J. D. Song, M.-C. Park, S. Im, D. K. Hwang, *Adv. Funct. Mater.* **2017**, *27*, 1703822.
- [51] T. V. Cuong, H. N. Tien, V. H. Luan, V. H. Pham, J. S. Chung, D. H. Yoo, S. H. Hahn, K.-K. Koo, P. A. Kohl, S. H. Hur, E. J. Kim, *Phys. Status Solidi A* **2011**, *208*, 943.
- [52] G. Li, M. Suja, M. Chen, E. Bekyarova, R. C. Haddon, J. Liu, M. E. Itkis, *ACS Appl. Mater. Interfaces* **2017**, *9*, 37094.
- [53] D. Y. Kim, J. Ryu, J. Manders, J. Lee, F. So, *ACS Appl. Mater. Interfaces* **2014**, *6*, 1370.
- [54] T. Xie, G. Liu, B. Wen, J. Y. Ha, N. V. Nguyen, A. Motayed, R. Debnath, *ACS Appl. Mater. Interfaces* **2015**, *7*, 9660.
- [55] D.-S. Um, Y. Lee, S. Lim, S. Park, H. Lee, H. Ko, *ACS Appl. Mater. Interfaces* **2016**, *8*, 33955.
- [56] Q. Hong, Y. Cao, J. Xu, H. Lu, J. He, J. L. Sun, *ACS Appl. Mater. Interfaces* **2014**, *6*, 20887.
- [57] S. Zheng, J. Lu, X. Duan, *ACS Omega* **2016**, *1*, 1239.
- [58] L. X. Zheng, P. Yu, K. Hu, F. Teng, H. Chen, X. S. Fang, *ACS Appl. Mater. Interfaces* **2016**, *8*, 33924.
- [59] H. Y. Chen, P. Yu, Z. Zhang, F. Teng, L. Zheng, K. Hu, X. S. Fang, *Small* **2016**, *12*, 5809.
- [60] M. Wang, Y. Lian, X. Wang, *Curr. Appl. Phys.* **2009**, *9*, 189.
- [61] I. Iatsunskyi, A. Vasylenko, R. Viter, M. Kempirski, G. Nowaczyk, S. Jurga, M. Bechelany, *Appl. Surf. Sci.* **2017**, *411*, 494.
- [62] A. A. Chaaya, M. Bechelany, S. Balme, P. Miele, *J. Mater. Chem. A* **2014**, *2*, 20650.
- [63] S.-W. Lee, S.-H. Cha, K.-J. Choi, B.-H. Kang, J.-S. Lee, S.-W. Kim, J.-S. Kim, H.-M. Jeong, S.-A. Gopalan, D.-H. Kwon, S.-W. Kang, *Sensors* **2016**, *16*, 74.
- [64] P. P. Yu, K. Hu, H. Chen, L. Zheng, X. S. Fang, *Adv. Funct. Mater.* **2017**, *27*, 1703166.
- [65] J. Malloys, M. Planells, V. Thakare, R. Bhosale, S. Ogale, N. Robertson, *ACS Appl. Mater. Interfaces* **2015**, *7*, 27597.
- [66] F. Meng, L. Shen, Y. Wang, S. Wen, X. Gu, J. Zhou, S. Tian, S. Ruan, *RSC Adv.* **2013**, *3*, 21413.
- [67] W. Tian, H. Zhou, L. Li, *Small* **2017**, *13*, 1702107.
- [68] Y. Chen, M. He, J. Peng, Y. Sun, Z. Liang, *Adv. Sci.* **2016**, *3*, 1500392.
- [69] X. Yi, Z. Ren, N. Chen, C. Li, X. Zhong, S. Yang, J. Wang, *Adv. Electron. Mater.* **2017**, *3*, 1700251.
- [70] Z. Zheng, F. Zhuge, Y. Wang, J. Zhang, L. Gan, X. Zhou, H. Li, T. Zhai, *Adv. Funct. Mater.* **2017**, *27*, 1703115.
- [71] F. Cao, W. Tian, B. Gu, Y. Ma, H. Lu, L. Li, *Nano Res.* **2017**, *10*, 2244.
- [72] M. Sun, Q. Fang, Z. Zhang, D. Xie, Y. Sun, J. Xu, W. Li, T. Ren, Y. Zhang, *ACS Appl. Mater. Interfaces* **2018**, *10*, 7231.
- [73] J. Sun, J. Wu, X. Tong, F. Lin, Y. Wang, Z. M. Wang, *Adv. Sci.* **2018**, *5*, 1700780.
- [74] L. Z. Hao, Y. J. Liu, Z. D. Han, Z. J. Xu, J. Zhu, *J. Alloys Compd.* **2018**, *735*, 88.
- [75] C. Ling, T. Guo, W. Lu, Y. Xiong, L. Zhu, Q. Xue, *Nanoscale* **2017**, *9*, 8848.
- [76] Y. Zhao, J. Zhang, D. Jiang, C. Shan, Z. Zhang, B. Yao, D. Zhao, D. Shen, *ACS Appl. Mater. Interfaces* **2009**, *1*, 2428.
- [77] H. Zhang, M. Zhang, C. Feng, W. Chen, C. Liu, J. Zhou, S. Ruan, *Appl. Opt.* **2012**, *51*, 894.
- [78] N. Liu, G. Fang, W. Zeng, H. Zhou, F. Cheng, Q. Zheng, L. Yuan, X. Zou, X. Zhao, *ACS Appl. Mater. Interfaces* **2010**, *2*, 1973.
- [79] M.-W. Chen, C.-Y. Chen, D.-H. Lien, Y. Ding, J.-H. He, *Opt. Express* **2010**, *18*, 14836.
- [80] F.-X. Liang, J.-Z. Wang, Y. Wang, Y. Lin, L. Liang, Y. Gao, L.-B. Luo, *Appl. Surf. Sci.* **2017**, *426*, 391.
- [81] B. Nie, J.-G. Hu, L.-B. Luo, C. Xie, L.-H. Zeng, P. Lv, F.-Z. Li, J.-S. Jie, M. Feng, C.-Y. Wu, Y.-Q. Yu, S.-H. Yu, *Small* **2013**, *9*, 2872.
- [82] H.-Y. Liu, W.-C. Sun, S.-Y. Wei, S.-M. Yu, *IEEE Trans. Electron Devices* **2016**, *63*, 2424.
- [83] S.-J. Chang, T.-Y. Tsai, Z.-Y. Jiao, C.-J. Chiu, W.-Y. Weng, S.-H. Wang, C.-L. Hsu, T.-J. Hsueh, S.-L. Wu, *IEEE Electron Device Lett.* **2012**, *33*, 1577.
- [84] M. Karbalaee Akbari, Z. Hai, Z. Wei, C. Detavernier, E. Solano, F. Verpoort, S. Zhuiykov, *ACS Appl. Mater. Interfaces* **2018**, *10*, 10304.
- [85] D. Zheng, J. Wang, W. Hu, L. Liao, H. Fang, N. Guo, P. Wang, F. Gong, X. Wang, Z. Fan, X. Wu, X. Meng, X. Chen, W. Lu, *Nano Lett.* **2016**, *16*, 2548.
- [86] B. Deka Boruah, A. Misra, *ACS Appl. Mater. Interfaces* **2016**, *8*, 4771.
- [87] Y. Jin, J. Wang, B. Sun, J. C. Blakesley, N. C. Greenham, *Nano Lett.* **2008**, *8*, 1649.
- [88] S. Thangavel, K. Krishnamoorthy, V. Krishnaswamy, N. Raju, S. J. Kim, G. Venugopal, *J. Phys. Chem. C* **2015**, *119*, 22057.
- [89] Z. Jin, Q. Zhou, Y. Chen, P. Mao, H. Li, H. Liu, J. Wang, Y. Li, *Adv. Mater.* **2016**, *28*, 3697.
- [90] S. Mitra, A. Aravindh, G. Das, Y. Pak, I. Ajia, K. Loganathan, E. Di Fabrizio, I. S. Roqan, *Nano Energy* **2018**, *48*, 551.
- [91] Z. Lou, G. Shen, *Adv. Sci.* **2016**, *3*, 1500287.
- [92] W. Tian, H. Lu, L. Li, *Nano Res.* **2015**, *8*, 382.
- [93] A. J. Molina-Mendoza, A. Moya, R. Frisenda, S. A. Svatek, P. Gant, S. Gonzalez-Abad, E. Antolin, N. Agraït, G. Rubio-Bollinger, D. Perez de Lara, J. J. Vilatela, A. Castellanos-Gomez, *J. Mater. Chem. C* **2016**, *4*, 10707.
- [94] L. Ren, T. Tian, Y. Li, J. Huang, X. Zhao, *ACS Appl. Mater. Interfaces* **2013**, *5*, 5861.
- [95] J. M. Wu, W. E. Chang, *ACS Appl. Mater. Interfaces* **2014**, *6*, 14286.
- [96] X. Zhou, Q. Zhang, L. Gan, X. Li, H. Li, Y. Zhang, D. Golberg, T. Zhai, *Adv. Funct. Mater.* **2016**, *26*, 704.
- [97] Z. He, Q. Liu, H. Hou, F. Gao, B. Tang, W. Yang, *ACS Appl. Mater. Interfaces* **2015**, *7*, 10878.
- [98] C. Gong, K. Hu, X. Wang, P. Wangyang, C. Yan, J. Chu, M. Liao, L. Dai, T. Zhai, C. Wang, L. Li, J. Xiong, *Adv. Funct. Mater.* **2018**, *28*, 1706559.
- [99] J. Li, Z. Wang, Y. Wen, J. Chu, L. Yin, R. Cheng, L. Lei, P. He, C. Jiang, L. Feng, J. He, *Adv. Funct. Mater.* **2018**, *28*, 1706437.
- [100] F. Wang, Z. Wang, T. A. Shifa, Y. Wen, F. Wang, X. Zhan, Q. Wang, K. Xu, Y. Huang, L. Yin, C. Jiang, J. He, *Adv. Funct. Mater.* **2017**, *27*, 1603254.
- [101] Z. Sun, T. Liao, Y. Dou, S. M. Hwang, M.-S. Park, L. Jiang, J. H. Kim, S. X. Dou, *Nat. Commun.* **2014**, *5*, 3813.
- [102] Z. Hai, M. K. Akbari, C. Xue, H. Xu, S. Depuydt, S. Zhuiykov, *Sens. Actuators, B* **2017**, *245*, 954.
- [103] Z. Hai, M. K. Akbari, C. Xue, H. Xu, L. Hyde, S. Zhuiykov, *Appl. Surf. Sci.* **2017**, *405*, 169.
- [104] W. Feng, X. Wang, J. Zhang, L. Wang, W. Zheng, P. Hu, W. Cao, B. Yang, *J. Mater. Chem. C* **2014**, *2*, 3254.
- [105] J. Wu, Y. Liu, Z. Tan, C. Tan, J. Yin, T. Li, T. Tu, H. Peng, *Adv. Mater.* **2017**, *29*, 1704060.
- [106] T. Goswami, A. Mondal, P. Singh, B. Choudhuri, *Solid State Sci.* **2015**, *48*, 56.
- [107] P. Sahatiya, C. S. Reddy K, S. Badhulika, *J. Mater. Chem. C* **2017**, *5*, 12728.
- [108] D. Ghosh, S. Kapri, S. Bhattacharyya, *ACS Appl. Mater. Interfaces* **2016**, *8*, 35496.
- [109] X. Liu, X. Ji, M. Liu, N. Liu, Z. Tao, Q. Dai, L. Wei, C. Li, X. Zhang, B. Wang, *ACS Appl. Mater. Interfaces* **2015**, *7*, 2452.

- [110] C. Chen, P. Zhou, N. Wang, Y. Ma, H. San, *Nanomaterials* **2018**, *8*, 26.
- [111] A. Saravanan, B. R. Huang, D. Kathiravan, A. Prasannan, *ACS Appl. Mater. Interfaces* **2017**, *9*, 39771.
- [112] X. Wang, K. Liu, X. Chen, B. Li, M. Jiang, Z. Zhang, H. Zhao, D. Shen, *ACS Appl. Mater. Interfaces* **2017**, *9*, 5574.
- [113] A. D. Mottram, Y.-H. Lin, P. Pattanasattayavong, K. Zhao, A. Amassian, T. D. Anthopoulos, *ACS Appl. Mater. Interfaces* **2016**, *8*, 4894.
- [114] W. X. Ouyang, L. Su, X. S. Fang, *Small* **2018**, *14*, 1801611.
- [115] D. H. Lien, J. R. Retamal, J. J. Ke, C. F. Kang, J. H. He, *Nanoscale* **2015**, *7*, 19874.
- [116] C.-Y. Chen, J. R. D. Retamal, I.-W. Wu, D.-H. Lien, M.-W. Chen, Y. Ding, Y.-L. Chueh, C.-I. Wu, J.-H. He, *ACS Nano* **2012**, *6*, 9366.
- [117] M.-W. Chen, J. R. D. Retamal, C.-Y. Chen, J.-H. He, *IEEE Electron Device Lett.* **2012**, *33*, 411.
- [118] C. H. Lin, D. S. Tsai, T. C. Wei, D. H. Lien, J. J. Ke, C. H. Su, J. Y. Sun, Y. C. Liao, J. H. He, *ACS Nano* **2017**, *11*, 10230.
- [119] C.-Y. Chen, M.-W. Chen, C.-Y. Hsu, D.-H. Lien, M.-J. Chen, J.-H. He, *IEEE J. Sel. Top. Quantum Electron.* **2012**, *18*, 1807.
- [120] Z. Guo, L. Zhou, Y. Tang, L. Li, Z. Zhang, H. Yang, H. Ma, A. Nathan, D. Zhao, *ACS Appl. Mater. Interfaces* **2017**, *9*, 31042.
- [121] F. Wang, Z. Wang, C. Jiang, L. Yin, R. Cheng, X. Zhan, K. Xu, F. Wang, Y. Zhang, J. He, *Small* **2017**, *13*, 1604298.
- [122] H.-Y. Chen, K.-W. Liu, X. Chen, Z.-Z. Zhang, M.-M. Fan, M.-M. Jiang, X.-H. Xie, H.-F. Zhao, D.-Z. Shen, *J. Mater. Chem. C* **2014**, *2*, 9689.
- [123] Z. Song, P. Wang, L. Guo, Y. Yang, Q. Tang, *Jpn. J. Appl. Phys.* **2015**, *54*, 052201.
- [124] Y. Cao, K. Cai, P. Hu, L. Zhao, T. Yan, W. Luo, X. Zhang, X. Wu, K. Wang, H. Zheng, *Sci. Rep.* **2015**, *5*, 8130.
- [125] J. Miao, S. Zhang, L. Cai, C. Wang, *Adv. Electron. Mater.* **2016**, *2*, 1500346.
- [126] Z. Zheng, L. Gan, J. Zhang, F. Zhuge, T. Zhai, *Adv. Sci.* **2017**, *4*, 1600316.
- [127] L. Li, Z. Lou, G. Shen, *Adv. Funct. Mater.* **2018**, *28*, 1705389.
- [128] B. Zhou, B. Shi, D. Jin, X. Liu, *Nat. Nanotechnol.* **2015**, *10*, 924.
- [129] M. L. Tsai, W. C. Tu, L. Tang, T. C. Wei, W. R. Wei, S. P. Lau, L. J. Chen, J. H. He, *Nano Lett.* **2016**, *16*, 309.
- [130] F. Teng, K. Hu, W. Ouyang, X. S. Fang, *Adv. Mater.* **2018**, *30*, 1706262.
- [131] Z. Wang, X. He, X.-X. Zhang, H. N. Alshareef, *Adv. Mater.* **2016**, *28*, 9133.
- [132] N. Oliva, E. A. Casu, C. Yan, A. Krammer, T. Rosca, A. Magrez, I. Stolichnov, A. Schueler, O. J. F. Martin, A. M. Ionescu, *Sci. Rep.* **2017**, *7*, 14250.
- [133] C. Xie, C. Mak, X. Tao, F. Yan, *Adv. Funct. Mater.* **2017**, *27*, 1603886.
- [134] X. Chen, G. Liu, Y. Hu, W. Cao, P. Hu, W. Hu, *Nanotechnology* **2018**, *29*, 045202.
- [135] L. Peng, L. Hu, X. S. Fang, *Adv. Funct. Mater.* **2014**, *24*, 2591.
- [136] S. F. Leung, K. T. Ho, P. K. Kung, V. K. S. Hsiao, H. N. Alshareef, Z. L. Wang, J. H. He, *Adv. Mater.* **2018**, *30*, 1704611.
- [137] C.-H. Lin, H.-C. Fu, D.-H. Lien, C.-Y. Hsu, J.-H. He, *Nano Energy* **2018**, *51*, 294.
- [138] D. Periyagounder, P. Gnanasekar, P. Varadhan, J.-H. He, J. Kulandaivel, *J. Mater. Chem. C* **2018**, *6*, 9545.
- [139] B. Zhao, F. Wang, H. Chen, L. Zheng, L. Su, D. Zhao, X. S. Fang, *Adv. Funct. Mater.* **2017**, *27*, 1700264.
- [140] M. Chen, B. Zhao, G. Hu, X. S. Fang, H. Wang, L. Wang, J. Luo, X. Han, X. Wang, C. Pan, Z. L. Wang, *Adv. Funct. Mater.* **2018**, *28*, 1706379.
- [141] B. Ouyang, K. Zhang, Y. Yang, *Adv. Mater. Technol.* **2017**, *2*, 1700208.
- [142] F. Liu, C. Zhu, L. You, S. J. Liang, S. Zheng, J. Zhou, Q. Fu, Y. He, Q. Zeng, H. J. Fan, L. K. Ang, J. Wang, Z. Liu, *Adv. Mater.* **2016**, *28*, 7768.
- [143] C. O. Chey, A. Masood, A. Riazanova, X. Liu, K. V. Rao, O. Nur, M. Willander, *J. Nanomater.* **2014**, *2015*, 222.
- [144] Y. Ning, Z. Zhang, F. Teng, X. S. Fang, *Small* **2018**, *14*, 1703754.
- [145] C. Xie, F. Yan, *Small* **2017**, *13*, 1701822.
- [146] C. Yan, J. Wang, X. Wang, W. Kang, M. Cui, C. Y. Foo, P. S. Lee, *Adv. Mater.* **2014**, *26*, 943.
- [147] Y. S. Rim, S. H. Bae, H. Chen, N. De Marco, Y. Yang, *Adv. Mater.* **2016**, *28*, 4415.
- [148] W. Yang, K. Hu, F. Teng, J. H. Weng, Y. Zhang, X. S. Fang, *Nano Lett.* **2018**, *18*, 4697.
- [149] X. J. Xu, S. Y. Li, J. X. Chen, S. Cai, Z. H. Long, X. S. Fang, *Adv. Funct. Mater.* **2018**, *28*, 1802029.
- [150] M. Qiu, P. Sun, Y. Liu, Q. Huang, C. Zhao, Z. Li, W. Mai, *Adv. Mater. Technol.* **2018**, *3*, 1700288.
- [151] X. Yu, Z. Zhao, J. Zhang, W. Guo, J. Qiu, D. Li, Z. Li, X. Mou, L. Li, A. Li, H. Liu, *Small* **2016**, *12*, 2759.
- [152] H. Y. Chen, K. Liu, L. Hu, A. A. Al-Ghamdi, X. S. Fang, *Mater. Today* **2015**, *18*, 493.
- [153] X. J. Xu, J. Chen, S. Cai, Z. Long, Y. Zhang, L. Su, S. He, C. Tang, P. Liu, H. Peng, X. S. Fang, *Adv. Mater.* **2018**, *30*, 1803165.